**DOKUZ EYLÜL UNIVERSITY**

**GRADUATE SCHOOL OF NATURAL AND APPLIED SCIENCES**

# IMPROVEMENT PHOTOCATALYTIC PROPERTIES OF DOPED NANOPARTICLES SYNTHESIZED BY SOL-GEL METHOD

**by**

**Sıla CENGİZ**

**October, 2019**

**İZMİR**

# IMPROVEMENT PHOTOCATALYTIC PROPERTIES OF DOPED NANOPARTICLES SYNTHESIZED BY SOL-GEL METHOD

**A Thesis Submitted to the**
**Graduate School of Natural and Applied Sciences of Dokuz Eylül University**
**In Partial Fulfillment of the Requirements for the Degree of Master of Science**
**in Nanoscience and Nanoengineering**

**by**

**Sıla CENGİZ**

**October, 2019**

**İZMİR**

**M.Sc THESIS EXAMINATION RESULT FORM**

We have read the thesis entitled **''IMPROVEMENT PHOTOCATALYTIC PROPERTIES OF DOPED NANOPARTICLES SYNTHESIZED BY SOL-GEL METHOD''** completed by **SILA CENGİZ** under supervision of **ASSIST. PROF. DR. FUNDA AK AZEM** and we certify that in our opinion it if fully adequate, in scope and in quality, as a thesis for the degree of Master of Science.

Assist. Prof. Dr. Funda Ak AZEM

Supervisor

Assoc. Prof. Dr. Hüsnügül Yılmaz ATAY

Assoc. Prof. Dr. Hüsnügül Yılmaz ATAY

Assist. Prof. Dr. Işıl BİRLİK

Assist. Prof. Dr. Işıl BİRLİK

Prof. Dr. Kadriye ERTEKİN

Director

Graduate School of Natural and Applied Sciences

## ACKNOWLEDGEMENTS

First of all, I would like to express to my sincere gratitude to my advisor Assist. Prof. Dr. Funda AK AZEM for her excellent guidance, patient supervision and continuous support thought the preparation of this study. I would also like to thank Assist. Prof. Dr. Işıl BİRLİK for helping me with my study and research.

I heartfully express my special thanks for my co-workers, Doğacan DAĞDELEN and Tülay KOÇ DELİCE for their support, help, patience and invaluable friendship. I also wish to thank Ramazan DALMIŞ, Özgür Yasin KESKİN, Dalyan ÖZKAN for their collaboration in the laboratory studies and sharing their valuable experiences with me. Additionally, I would like to thank Şükrü KAYA and Serhan KÖKTAŞ, Çağrı KILINÇ for their friendships and supports.

Finally, I would like to express my deepest thanks to my family Celal CENGİZ, Sultan CENGİZ and Andaç Baran CENGİZ who always believed and supported me no matter the circumstances. This thesis work was easier with their presence in my life.

Sıla CENGİZ

**IMPROVEMENT PHOTOCATALYTIC PROPERTIES OF DOPED NANOPARTICLES SYNTHESIZED BY SOL-GEL METHOD**

## ABSTRACT

Among the transition metal oxide semiconductors, titanium dioxide is the most suitable photocatalyst commonly used for photocatalysis applications. However, there are still many difficulties to enhance the photocatalytic performance of titanium dioxide. Various techniques have been applied to develop the photocatalytic properties of titanium dioxide nanoparticles, such as doping transition metal elements (Ag, Ni, Cu, Zn etc.) doping, rare earth metal elements (La, Ce, Eu etc.) doping to other metals and non-metals elements (F, C, S etc.). Titanium dioxide is compatible with transition metal cations such as chromium, which has a high absorption of visible light. Scientific research shows that the doping of a transition metal and a noble metal together into titanium dioxide structure may lead to the development of photoactivity.

The present thesis involves, pure chromium doped, chromium and nitrogen codoped $TiO_2$ nanoparticles production by a sol-gel method using titanium(IV) isopropoxide, chromium nitrate and urea as precursors.

Structural characterization of the undoped and doped $TiO_2$ nanoparticles was performed by X-ray diffraction (XRD), Fourier transform infrared spectroscopy (FTIR) and X-ray photoelectron spectrometry (XPS). Particle size measurements of nanoparticles were performed by using Zetasizer. XRD results show that the undoped, Cr doped and Cr/N codoped $TiO_2$ nanoparticles have the anatase phase. The photocatalytic properties of synthesized nanoparticles were determined by degredation of methylene blue solution under UV illumination. Photocatalytic efficiency of undoped, doped and codoped $TiO_2$ were compared. The best photocatalytic activity was observed in C/N codoped $TiO_2$ nanoparticles.

**Keywords:** Nanoparticles, sol-gel, nitrogen, chromium, photocatalytic activity

# SOL-JEL YÖNTEMİ İLE SENTEZLENEN KATKILI NANOPARTİKÜLLERİN FOTOKATALİTİK ÖZELLİKLERİNİN GELİŞTİRİLMESİ

## ÖZ

Titanyum dioksit, geçiş metal oksit yarı iletkenleri arasında, fotokataliz uygulamaları için yaygın olarak kullanılan en uygun fotokatalisttir. Bununla birlikte, $TiO_2$'nin fotokatalitik aktivitesini arttırmak için hala birçok zorluk bulunmaktadır. $TiO_2$'nin fotokatalitik aktivitesini geliştirmek için, geçiş metalleri (Ag, Ni, Cu, Zn vb.), nadir toprak elementleri (La, Ce, Eu vb.), ametaller (F, C, S vb.) ve diğer metallerin katkılanması gibi çeşitli teknikler uygulanmıştır. $TiO_2$, görülebilir ışıkta yüksek emilimine sahip $Cr^{3+}$ gibi geçiş metal (TM) katyonları ile uyumlu olmaktadır. Son zamanlarda yapılan çalışmalar, bir metalin ve bir ametalin $TiO_2$'ye birlikte katkısının görünür aktif fotokatalizörlerin gelişimine yol açabileceğini göstermektedir.

Tez çalışması, saf, krom katkılı, krom ve azot eş katkılı $TiO_2$ nanopartiküllerinin, başlangıç malzemeleri olarak sırasıyla titanyum (IV) izopropoksit, krom nitrat ve üre kullanılarak sol-jel yöntemi ile hazırlanmasını içermektedir.

Katkısız ve katkılı $TiO_2$ nanopartiküllerin yapısal karakterizasyonu X-ışını difraksiyonu (XRD), Fourier Transform Infrared spektroskopisi (FTIR) ve X-ışını Fotoelektron Spektrometresi (XPS) ile gerçekleştirilmiştir. Nanopartiküllerin partikül büyüklüğü ölçümleri için Zetasizer kullanılmıştır. XRD sonuçları, katkısız, Cr katkılı ve Cr/N eş katkılı $TiO_2$ nanopartiküllerinin anataz fazına sahip olduğunu göstermektedir. Sentezlenen nanopartiküllerin fotokatalitik özellikleri, UV ışığı altında metilen mavisi çözeltisinin degredasyonu ile belirlenmektedir. Katkısız, katkılı ve eş katkılı $TiO_2$ nanopartiküllerinin fotokatalitik etkinliği karşılaştırılmaktadır. En iyi fotokatalitik aktivite C/N eş katkılı $TiO_2$ nanopartiküllerinde gözlemlenmiştir.

**Anahtar kelimeler:** Nanopartikül, sol-jel, nitrojen, krom, fotokatalitik aktivite

**CONTENTS**

**Page**

**LIST OF FIGURES**

**Page**

## LIST OF TABLES

**Page**

# CHAPTER ONE
# INTRODUCTION

The word "nano" is becoming increasingly common in the scientific literature. Nano is derived from "nanos", which means "dwarf" in Greek. Recently, many "nano" prefixed words that have not yet been fully recognized have been used in science publications. For example; nanometer, nanoscience, nanotechnology, nanostructure, nanoparticle, nanotube (Buzea, Pacheco & Robbie, 2007).

Researchers have carried out studies on the preparation of ceramic nanoparticles that exhibit new and interesting properties compared to other materials. Ceramic nanoparticles ($TiO_2$, ZnO, $Al_2O_3$, $CeO_2$, $Fe_2O_3$, $Fe_3O_4$, $SiO_2$) are considered to be one of the most attractive nanomaterials. $TiO_2$ is of great interests recently due to its unique properties such as wide band gap under UV light, superior mechanical toughness, high photocatalytic activity. $TiO_2$ has attractive optical, dielectric and catalytic properties for some applications such as self-cleaning, non-fogging surfaces, photochemical cancer treatment applications, air purification, dye materials, sensors, photocatalysts (Dalvandi & Ghasemi, 2013).

Various techniques have been used to synthesize titanium nanoparticles such as the inert gas condensation, sol-gel technique, chemical vapor deposition, spray pyrolysis and others by controlled nucleation and growth processes. Among the production techniques, the sol-gel technique appears to be the preferred method because of its excellent chemical homogeneity and low cost at low reaction temperatures (Dalvandi & Ghasemi, 2013).

Photocatalysts are structures that exhibit photoactive properties when stimulated by UV light. $TiO_2$ is a semiconductor material that exhibits photocatalyst properties and can also decompose organic groups. Photocatalytic reaction; is known as electrochemical energy transfer of light energy of photons through a catalyst (Paleaz et al., 2012).

The fact that $TiO_2$ can be activated by UV light, which forms only a small part of the solar spectrum, limits the use of this material in practical applications. In addition, the band gap of $TiO_2$ has a limiting effect for use in practical applications. The band gap of $TiO_2$ is 3.2 eV. Therefore, for practical applications, the photoactivity of $TiO_2$ needs to be improved. There are many studies in the literature on the development of photoactivity (Lee, Hong & Mohseni, 2005). One way to increase the photoactivity is to shift the absorption band from the UV region to the visible region by doping $TiO_2$ with transition metals and noble metals (Zhang, Liang, Wu & Zheng, 2012).

To further increase the photoactivity of $TiO_2$, the simultaneous doping of nonmetal and metal oxide atoms have become the focus of many researchers. In addition, it may result in improved photocatalytic efficiency and other properties compared to single doped $TiO_2$ (Yamamoto, 2002).

In this study, we synthesized undoped, Cr doped, Cr/N codoped anatase $TiO_2$ nanoparticles for photocatalytic applications using sol-gel method. As a result of our literature research, it has been observed that chromium is a promising metal oxide additive so that chromium atoms are comparable in atomic size with titanium atoms and can easily be displaced (Samokhvalov, 2017). For this reason, chromium and nitrogen were selected as suitable dopants and codoping process was applied.

The structure of this thesis consists of five different chapters which are summarized below:

Chapter 2 is a literature review of nanomaterials, nanoparticles, doping and codoping mechanism, production techniques. Sol-gel technique was reviewed in detail as this work is connected to sol-gel synthesis.

Chapter 3 is a literature review of photocatalytic mechanism, photocatalytic properties, $TiO_2$ nanoparticles as catalyst. The photocatalytic properties are examined in detail in this study.

Chapter 4 is on the experimental work conducted, including preparation of undoped, doped and codoped nanoparticles and characterization techinques.

Chapter 5 presents results and discussions, including particle size measurements of nanoparticles, XRD, XPS, FT-IR and photocatalytic properties results of undoped, Cr doped and Cr/N codoped $TiO_2$ nanoparticles.

Chapter 6 reviews the main conclusions of the study.

# CHAPTER TWO
# NANOMATERIALS

## 2.1 Classification of Nanomaterials

Nanotechnology encompasses the techniques of manipulation of the nano sized structure to develop a product with new properties, such as superior mechanical properties and durability. Nanotechnology covers the applications of nanostructured materials such as physical, synthetic, electronic, photocatalytic. Therefore, it is used in physics, chemistry and engineering (Ramsden, 2009).

Nanostructured materials typically have an average particle size of several nanometers, less than 100 nm. These materials are single-stage or multi-stage polycrystalline solids. Due to their unique microstructures, such materials display properties that are superior to conventional coarse-grained materials. Very small nanoparticles have more atoms in their particle boundaries than large ones. Therefore, since the crystal structures of the material are different, they can be depicted with many different interfaces (Suryanarayana, 1995). Nanomaterials with small particle size have very different and exceptional properties compared to other materials. For example; self-cleaning, low electrical resistivity. Besides, nanomaterials includes catalysts, energy conversion, sensors and biomedical applications (Suryanarayana, 2005).

The size classification applies to nanomaterials below 100 nm. Nanomaterials can be found in 3 types in terms of size classification. These; zero dimensional (0D), one dimensional (1D), two dimensional (2D) and three dimensional (3D) materials (Schodek, Ferreira & Ashby, 2009). 0D, 1D, 2D, 3D nanomaterials and shapes are available in Figure 2.1.

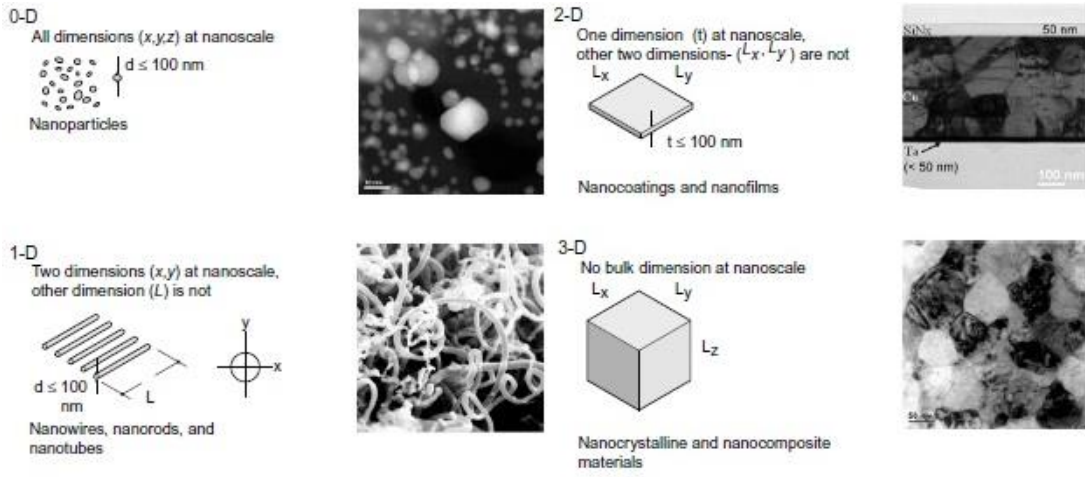


Figure 2.1 0D, 1D, 2D, and 3D nanomaterials shapes and sizes (Schodek et al., 2009)

Zero-dimensional nanomaterials are materials in which all measurements are estimated on a nanoscale. The most well-known portrayal of zero-dimensional nanomaterials are nanoparticles. Nanoparticles are the essential part of nanotechnology (Hasan, 2015). Nanoparticles have remarkable unique properties due to their dimension. These properties can be a relatively large surface area, expanded reactivity. These properties of nanoparticles have prompted the utilization of different applications (Smita, Gupta, Bartonova, Dusinska, Gutleb & Rahman, 2012).

Nanoparticles can be of different shapes, sizes and structures. Nanoparticles can be circular, barrel shaped or cone shaped (Machado, Pacheco, Nouws, Delerue & Albergaria, 2015). Various strategies for combination are being created to improve properties and diminish generation costs. These strategies are intended to improve the some properties (optical, mechanical etc ) of nanoparticles. (Choi, Holback, Liu, Park, Yeo & Abouelmagd, 2013).

Although free electrons are present, they have a structure that is limited in all three directions and the structures that are not mobile are called 0D (zero dimensional) structures. 0D nanomaterials are materials that are isolated from each other in the form of nanotose or nanodispersion. Today, these materials are available in many different forms and are synthesized by various research groups. Nanotope, quantum dots and

lumps are of this class. Such structures are necessarily used in many electronic functional applications, including quantum computers (Schodek et al., 2009).

Materials that have the ability of free electrons to move in one direction are called 1D (one dimensional) structures. Structures such as nanowire and nanotube are the structures in this group. Nanotubes have been discovered by Iijima and are increasingly gaining importance today. 1D nanomaterials are widely used in nanoelectronics, nanosystems, nano-devices and nanocomposites, alternative energy sources and national security fields (Schodek et al., 2009).

If free electrons can only move in two directions, then the material is a 2D material. All layered structures are two dimensional materials. In layered structures, one layer consists of one kind of atom and another layer consists of a different kind of atom. 2D materials are nanometric films and coatings. Today, 2D materials are gaining importance and their usage areas are increasing. The discovery of 2D materials began with graphene, followed by many materials such as boron nitride and molybdenum disulfide (Schodek et al., 2009).

Nano materials, whose free electrons can move axially in all three directions, are called 3D (three dimensional) structures, known as solids. 3D materials are powdered, fibrous, multi-layered and polycrystalline. The electronic properties and electronic functions of materials are directly related to their size. A material of any size may not be the only construction example. For example, the bismuth element has three different types of nanowires in one dimension. (Schodek et al., 2009).

## 2.2 Nanoparticles

### *2.2.1 Metal Based Nanoparticles*

Metal-based nanoparticles are synthesized from metals by bottom-up and top-down methods. Metal-based nanoparticles can be produced using metals such as aluminum (Al), chromium (Cr), nickel (Ni), gold (Au), bismuth (Bi), silicon (Si) and tungsten (W). The surface area increases as the particle size of the nanoparticles decreases. The

nanoparticles having a particle size between 1 and 100 nm have a large surface area. Metal nanoparticles can be used in chemistry, physics, medicine, environment applications due to their superior properties such as self-cleaning, biocompatibility, transient magnetism, low electrical resistance, electron trapping effect specific to their size (Salavati, Davar & Mir, 2008).

### *2.2.2 Ceramic Based Nanoparticles*

Ceramic nanoparticles are inorganic structures in which the ideal size and permeability properties can be configured effectively. There has been great interest in the use of ceramic nanoparticles in textile, pharmaceutical, engineering and environmental applications recently. Important studies have been conducted to investigate ceramic nanoparticles (Thomas, Sharma, Mishra & Talegaonkar, 2015).

Ceramic nanoparticles, such as aluminum oxide $Al_2O_3$, amorphous silica $SiO_2$, iron oxide $Fe_2O_3$, magnetite $Fe_3O_4$, titanium dioxide $TiO_2$, zirconium oxide $ZrO_2$, are synthesized to improve certain properties of materials. These nanoparticles have better properties in terms of reactivity and efficiency than metal based nanoparticles (Tai, Tai, Chang & Liu, 2007).

#### *2.2.2.1 $TiO_2$ Nanoparticles*

$TiO_2$ is an n-type semiconductor widely used in technological applications like self-cleaning, water purification and solar cells. $TiO_2$ has attractive optical, dielectric and catalytic properties. It is non–toxic, inexpensive, stable and it has high oxidative power owning to its electronic structure. However, exploiting the oxidative properties of $TiO_2$ has been limited because of its wide bandgap (3.2 eV) that mostly absorbs the UV region. Thus, it is important to understand the structural, optical and chemical properties. That is why it has attracted great attention recently by researchers (Dalvandi & Ghasemi, 2013). Titanium dioxide is also used in various environmental applications due to its very good photocatalytic property. Thanks to the photocatalytic property, unwanted organic substances are separated from water and air and pigments, fillers and photocatalysts are produced (Macwan & Dave, 2011).

$TiO_2$ may exist in three different crystal forms. These; anatase (tetragonal, a = b = 3.782Å, c = 9.502Å), rutile (tetragonal, a = b = 4.854Å, c = 2.953Å) and brookite (rhombohedral, a = 5.436Å, b = 9.166Å, c = 5.135Å) (Bagheri, Shameli & Hamid, 2012). The structure of anatase, rutile and brookite are shown in Figure 2.2. Each crystal form has different structures.

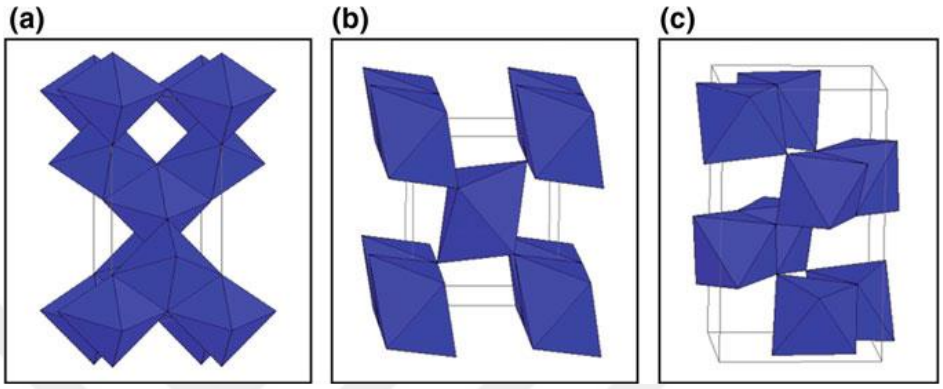


Figure 2.2 $TiO_2$ crystal forms (a) anatase, (b) rutile (c) brookite (Ullattil & Periyat, 2017)

Bagheri et al. synthesized anatase titanium dioxide nanoparticles by a sol-gel tecnique. They concluded that the nanoparticles in the anatase phase had the highest photocatalytic performance compared to other phases because of the large surface area per unit mass and volume (Bagheri et al., 2012). Martin et al. observed that $TiO_2$ nanoparticles in the form of anatase calcined at 400 °C had the best photodegredation rate (Martin, Morrison & Hoffmann, 1994). In another study, Peral et al. have shown that $TiO_2$ in anatase form is a better catalyst than other $TiO_2$ forms (Peral, Domenech & Ollis, 1997).

### *2.2.3 Carbon based nanoparticles*

Graphene and carbon nanotubes (CNT) are the most commonly used types of carbon-based nanoparticles (Bhaviripudi et al., 2006). Graphene and carbon nanotube structures are shown in the Figure 2.3.

Graphene is the first discovered 2D nanomaterials. Graphene is the separation of multi-layer graphite layers in which carbon atoms are arranged in a honeycomb structure. The reasons why graphene is so popular are its unique properties. It is a very

light material, one hundred times stronger than steel, its electrical conductivity is very high, it is 97% transparent when it is single layer and it is flexible 20%. The reason why graphene is so strong is its molecular structure consisting of carbon-carbon double bonds, and this bond is one of the strongest bonds in nature. Thus, the use of graphene in lead-proof materials is common. Graphene oxide and graphene with different atoms are also frequently used in the defense industry and recyclable energy sources.

Carbon nanotubes (CNT) are graphene folded and shaped into a tube. Single-layer and multi-layer carbon are separated into nanotubes. CNTs can be quite long despite their very thin diameters. CNTs are light and flexible materials with high electrical conductivity and high mechanical strength. CNTs are frequently used both in the health sector and in alternative energy sources. As a catalyst in implant materials, biosensors, energy sources and in the construction of artificial muscles, their robust and flexible structures make CNTs one of the most suitable candidates.

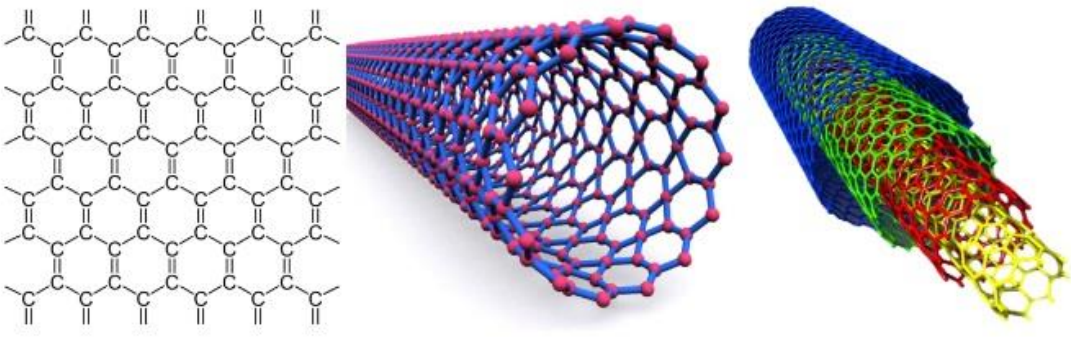

Figure 2.3 Graphene, single layer carbon nanotube and multilayer carbon nanotube molecule shapes (Ravi, Sharma & Parashar, 2019)

### *2.2.4 Doping Mechanisms of Nanoparticles*

In order to improve the properties of the nanoparticles, the surface properties can be adapted with the surface modification technique. The another technique, chemical modification can be done by adding a new catalyst or a new material to the material (Mallakpour & Madania, 2015).

In recent years, the doping method has attracted the attention of many scientists. Basically, the doping method can be described as the addition of another metal or nonmetal elements to the crystal structure of the nanoparticle. With the doping method, many changes can occur in the crystal structure, electro conductivity, surface area and particle size of the nanoparticle (Pelaez et al., 2012).

Band gap of semiconductor materials can be adjusted by the elemental contribution. The doping process is an effective method to accelerate and increase the photo activities of the semiconductors. Dopant atoms act as lattices for the scattering of electrons during the formation of photocatalytic reactions. This prevents recombination and increases photocatalytic efficiency. Many studies have been reported on the contribution of non-metal and metal elements to the structure of titanium dioxide. There are also many studies on the codoping of metal and non-metal elements (Zhang, Liang, Wu & Zheng, 2012). It is known that photocatalytic performance is increased by the contibution of noble metal to the structure of semiconductor nanoparticles (Lee et al., 2005).

Additionally, the contribution of non-metal elements such as N, F, S, P, C to the titanium dioxide structure is accepted as an effective approach to increase the photocatalytic efficiency in the ultraviolet (UV) region (Zaleska et al., 2008). Nitrogen (N) is accepted as the most promising dopant among non-metal elements (Emeline et al., 2007). When a single N contribution is applied to the titanium dioxide structure, charge unbalance occur. This has a negative effect on photocatalytic activity. Therefore, to overcome these limitations, many studies have been recorded on the codoping of transition metals and non-metal elements. It is known that transition metals such as Fe, Cr, Co, Mo, V, Mn increase the photocatalytic activity of titanium dioxide and reduce the recombination rate by creating surface defects (Choi, Termin & Hoffmann, 1994). Therefore, the codoping of transition metals and non-metal elements to the structure of titanium dioxide has become the focus of many researchers (Yamamoto, 2002).

Alvarez at al. synthesized Cr doped $TiO_2$ nanoparticles by microwave sol-gel tecnique. They observed that Cr doped $TiO_2$ had a lower particle size and reported an increase in photocatalytic efficiency compared to undoped nanoparticles (Alvarez et al., 2019). In another research, Alvarez et al. reported Cr doped $TiO_2$ (0.04 wt% Cr) catalyst is higher photocatalytic efficiency than the undoped $TiO_2$. The degradation rate of MCPA (4-chloro-2-methylphenoxyacetic acid) under UV and visible light was examined. The results were found to be related to the chemical structure, surface and optical properties of Cr doped $TiO_2$ nanoparticles (Alvarez, Mar, Palomino, Alejandro, Ramirez & Reyes 2017).

Deng et al. synthesized Mn doped $TiO_2$ nanoparticles by sol-gel method. Mn doped $TiO_2$ nanoparticles have been reported to have higher degradation rate than other samples (Deng, Xia, Guo, Gao & Shao 2011). In addition, Iwasaki et al. reported that the optical properties of Co doped $TiO_2$ nanoparticles were improved with measurements under UV irradiation (Iwasaki, Hara, Kawada, Taday & Ito, 2000).

### *2.2.5 Codoping Mechanisms of Nanoparticles*

The simultaneous doping method of two atoms has recently attracted the attention of many researchers (Pelaez et al., 2012). The aim of codoping process is to further increase the optical, electrical, or structural efficiency of nanoparticles compared to single doped nanoparticles (Cong, Zhang, Chen, Anpo & He, 2007).

This method is the result of the interaction of the two main structures. The acceptor additive is called 'A'. The donor additive is called 'D'. The examination of the steps of codoping method is as follows.

(i) The additives A and D react with each other to provide energy recovery.
(ii) As shown in Figure 2.4, these reactions allow the passage of electrons from A to D. This creates new energy levels. Thus, load balance is formed in addition to energy recovery (Yamamoto, 2002).

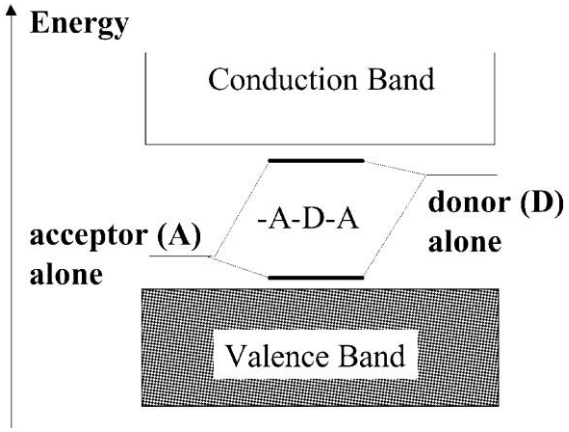


Figure 2.4 Formation of new energy levels by codoping method (Yamamoto, 2002)

Sun et al. synthesized Ag/N codoped and N doped $TiO_2$ nanoparticles by an acid-catalysed sol–gel process. The aim of this study was to increase the photocatalytic yield of nanoparticles. Increased photocatalytic performance of Ag / N codoped nanoparticles compared to single doped nanoparticles has been reported (Sun et al., 2013). Wang et al. observed that Co / N codoped $TiO_2$ nanoparticles had higher dye degradation rate than undoped $TiO_2$ nanoparticles. Thus, photocatalytic efficiency is increased (Wang, Zhao, Wang, Li & Li, 2015). Cong et al. observed that the photocatalytic performance of N / Fe codoped $TiO_2$ nanoparticles was improved compared to N single doped $TiO_2$ (Cong et al., 2007). Jia et al. observed a significant increase in photocatalytic performance of N and S codoped $TiO_2$ nanoparticles compared to N single doped and S single doped $TiO_2$ nanoparticles (Jia et al., 2011).

## 2.3 Synthesis Techniques of Nanomaterials

Materials scientists are researching about to production new materials with better functions, preferable capacities and lower costs. Different physical and compound techniques have been created to have better authority over molecule size and molecule dissemination. These methods also increase the performance of nanomaterials (Shibata, Aoki, Yano & Yamane, 1998).

There are two different ways of synthesizing nanomaterials. These are: top-down, bottom-up. Top down means bulk reduction applications from bulk material, whereas bottom-up material synthesis builds structure from atomic level (Hahn, 1997).

Top-down ways are incorporated into the ordinary solid – state handling of the materials. Along these ways depends on mass material. It makes the material little, so bigger particles are cleaved by the utilization of physical procedures, for example, pounding and granulating. For the most part, this way isn't appropriate for preparing homogeneously formed materials. Because of the high energy consumption, even very small particles are very difficult to production. The most serious issue with top-down methodology is the defects in the surface. These defects significantly affect the shaping and properties of nanostructures and nanomaterials. The customary top-down system can cause noteworthy crystallographic harm to the prepared models (Hahn, 1997).

The bottom up way performs to the accumulate of a material for production. Along these way is used more frequently in the preparation of most nano-scale materials with a uniform size and shape. It successfully includes synthetic amalgamation. It exactly controlls the process to prevent further molecule development. This method continues to be used today for the production of nano-sized structers (Figure 2.5) (Hahn, 1997).

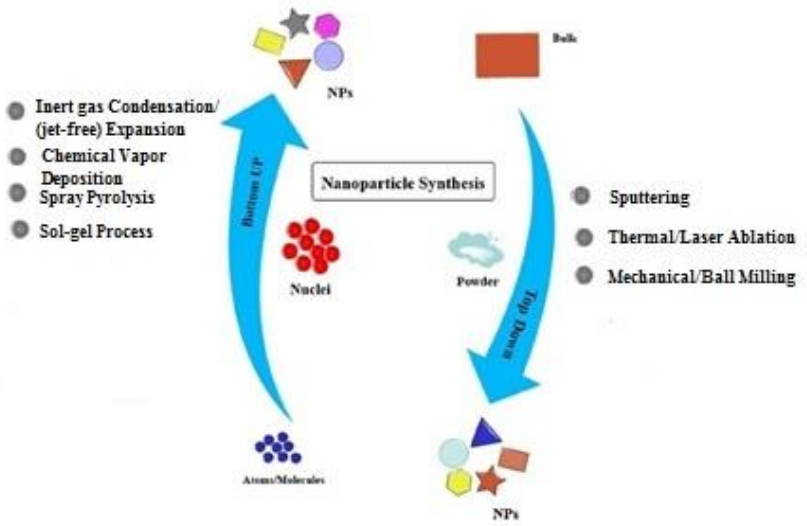


Figure 2.5 Top-down and bottom-up production methods of nanoparticles (Ovais et al., 2017)

### *2.3.1 Inert Gas Condensation*

In inert gas condensation is carried out by the removal of inorganic substances with the help of a gas (ordinarily argon, helium). Once the molecules boil, they slow down when they are in the same environment as the gas. After cooling the process with liquid nitrogen, particles of size 2 - 100 nm are collected on a finger. In this method, the particles tend to increase their clustering and size as they form. To avoid this, the process parameters must be carefully checked. The disadvantage of this method is; metallic and ceramic materials synthesized by this method are only laboratory-scale and mass structuring is difficult because the method is very slow (Schodek et al., 2009).

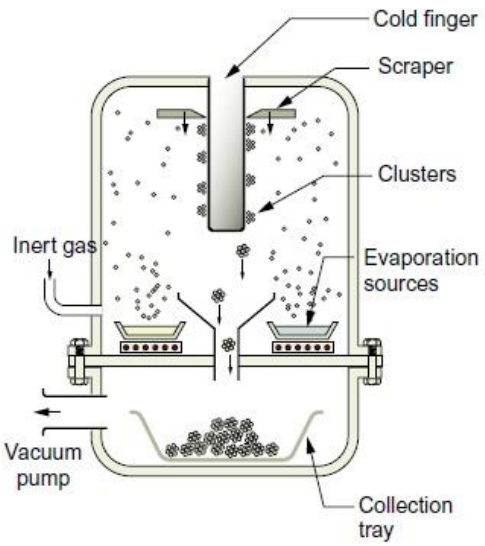


Figure 2.6 Schematic representation of the inert gas condensation method (Schodek et al., 2009)

### *2.3.2 Inert-gas (free-jet) Expansion*

In inert gas or free-jet expansion, the vaporized molecules are transported from a nozzle into a low pressure chamber with high pressure helium gas flow at supersonic speeds. The adiabatic spread of the gas causes a sudden cooling. Vaporized atoms thus form nanoparticles of a size of several nm. The density and quantity of gas entering the process must be carefully checked. Because the agglomeration of nanoparticles is the factor that determines the particle size and distribution (Schodek et al., 2009).

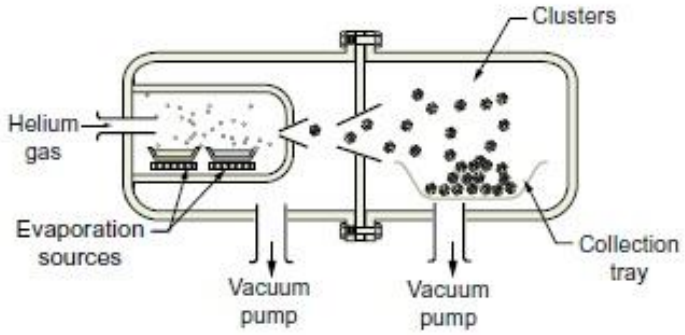


Figure 2.7 Sections of the system used and synthesis of nano clusters (Schodek et al., 2009)

### *2.3.3 Chemical Vapor Deposition (CVD)*

In the chemical vapor deposition method, the material surface is first heated in a closed container. The carrier gas then reacts to form a solid material. This solid material covers the material surface in a thin layer. This process is called chemical vapor deposition method. The CVD method is based on producing a solid phase coating material from the vapor phase in an environment with pressure set to the desired values. Coating thickness is thinner than 10 micrometers. The coating temperature varies according to the type of coating. It is generally between 500 and 1100 °C. Processing time also varies according to the type of coating (Kim, Okuyama, Nakaso & Shimada, 2004). Coating stoichiometry, morphology, chemical structure can be controlled by changing the parameters makes this method advantageous (Sudarshan, 2003).

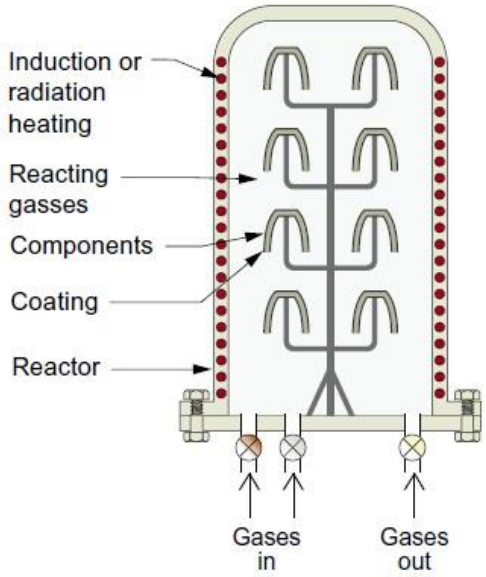


Figure 2.8 Production stages of chemical vapor deposition tecnique (Schodek et al., 2009)

### *2.3.4 Spray Pyrolysis*

In this method, purified leach solutions of high purity metal salts or secondary raw materials are used (Gürmen, Stopic & Friedrich, 2006). The process comprises the formation of discrete droplets from the initial solution in aerosol form, the realization of thermal disintegration, and the control of phase change. The aerosol can be easily generated ultrasonic by directing the high frequency (100 kHz-10 MHz) ultrasonic wave to the gas liquid interface (Tsai, Song, Tsai, Yang, Chiu & Lin, 2004). When the aerosol vapor enters the high temperature area (above 200°C), evaporation / drying, precipitation and disintegration of the droplet occurs at the droplet level.

The particle size thus formed is influenced by process parameters such as droplet size, structure of the initial solution used, temperature and time. After completion of the precipitation process, the temperature - time profile affects the particle growth that will occur in the other process steps of the spray pyrolysis process (Messing, Zhang & Jayanthi, 1993).

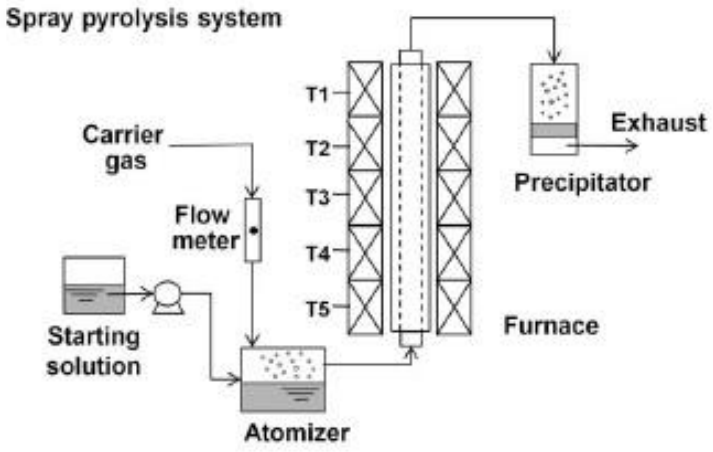


Figure 2.9 Schematics of a spray pyrolysis system (Overney, 2010)

### *2.3.5 Laser Ablation Synthesis*

Laser ablation (LAS) is a typical technique for nanoparticle generation from different solvents. The illumination of a metal submerged in a fluid solution by a laser bar gathers a plasma irradiation. This method is a solid top-down strategy. However, high cost of this method made LAS method used in only laboratory scale. In the LAS method, synthesis can be made without the need for any chemicals. A stable synthesis can be made with organic solvents and nanoparticles in water. Therefore it is known as a 'green' process (Amendola & Meneghetti, 2009).

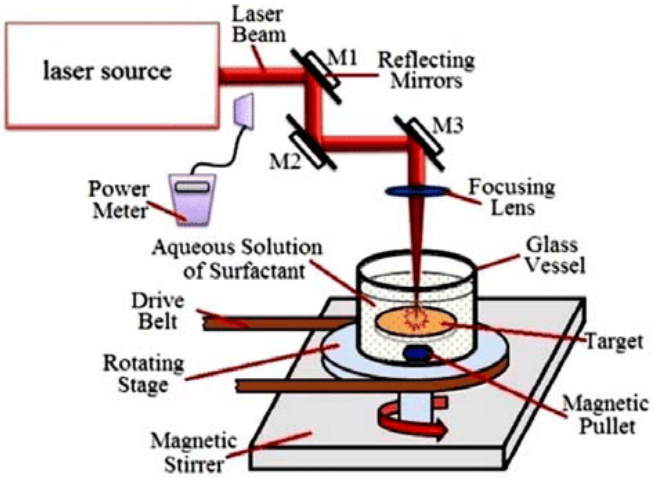


Figure 2.10 Mapping experimental set up of laser ablation method (Mahmoud, Fadhill & Al-nassar, 2013)

### *2.3.6 Mechanical Milling*

Milling, shown in Figure 2.11, combines two different particles that won't blend regularly. The particles are crushed and shredded by two large metal balls. Theese particles are flattened, welded, separated. The balls get the particles among them and pulverize. Theese method (if continued for a long time) produces heavily deformed particles with a nanoscale internal structure. In order to limit the surface roughness that occurs during the welding process, the system is filled with inert gas which assists in cooling (Schodek et al., 2009).

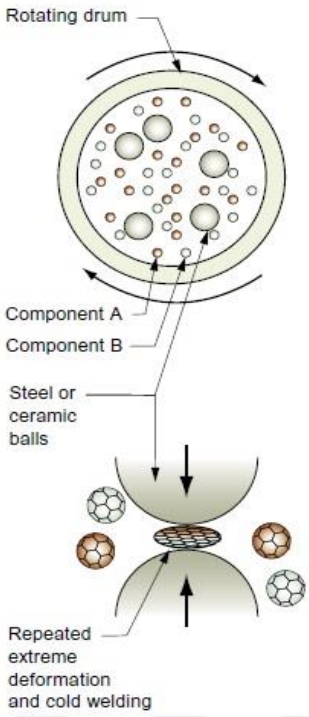

Figure 2.11 Powder milling with mechanical alloying (Schodek et al., 2009)

### *2.3.7 Sol-Gel Technique*

Synthesising environmentally friendly economic nanomaterials, with inspect over particle size, morphology, purity, amount and quality. The decision of production system might be a significant factor in deciding the relevance of the research (Hahn, 1997). This research focuses on sol-gel processing and characterization techniques.

The sol-gel procedure is a flexible generation technique for making ceramic and glass materials (Xu & Anderson, 1994). By and large, the sol-gel procedure includes the change of a framework through a fluid 'sol' in a colloidal structure, which is regularly changed over to strong gel-stage (Feinle, Elsaesser & Hüsing, 2016).

The steps in sol-gel procedure are as per the following: (Woodhead & Segal, 1984).

- Preparation of a homogeneous solution.
- By adjusting the hydrolysis conditions and adding additives, it is possible to control the particle size and provide product-specific properties by the operations carried out at the molecular level.

- Transformation from sol phase to gel phase by polymerization and condensation methods. This transformation can prompt various applications in the field of industrial and science.
- Aging
- Drying
- Calcination (Kakihana, 1996).

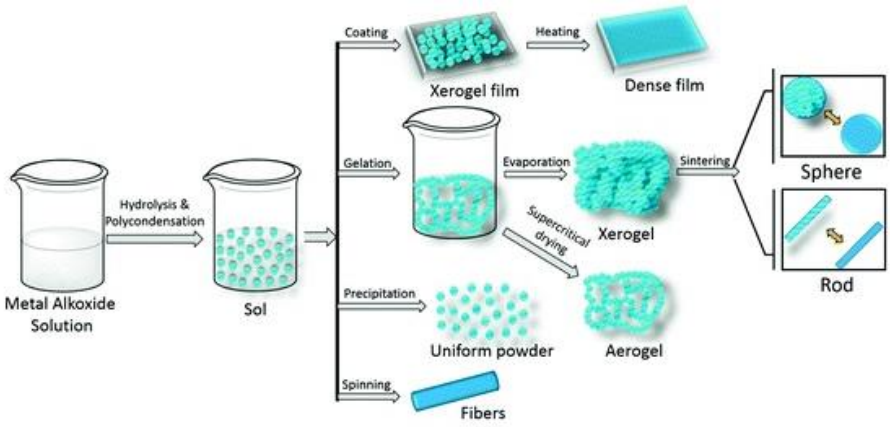


Figure 2.12 Schematic portrayal of sol–gel synthesis (Ullattil & Periyat, 2017)

Any starting chemicals may be used as long as it is miscible in the appropriate solvent. They are grouped under 2 main groups; metal salts and alkoxides. The main equation of metallic salt is $M_nX_n$ (M is metal, X an anionic group). Example: Aluminum $AlCl_3$. The formula of the alkoxides is $M(OR)_n$. M = cation ROH: alcohol group. Example: Aluminum ethoxide, $Al(OC_2H_5)_3$ (Pierre, 1998).

Alkoxides and metal salts have a same structure, so that their hydrolysis is similar. During the hydrolysis reactions, the alkoxy groups (OR) are changed by hydroxo ligands (OH) or oxo (O) ligands. The factors affecting hydrolysis are shown as follows;

- Properties of the alkyl group
- Feature of solvent
- Concentration of each component used in solvent
- Water / Alkoxide molarities ratios ($r_w = [H_2O] / [alk.]$
- Temperature

The reactions of $TiO_2$ with water as well as hydrolysis and condensation reactions are given specified (Pierre, 1998).

$$[M(OH_2)_N]^{z+} + hH_2O \rightarrow [M(\underline{OH})_h(OH_2)_{N-h}]^{(z-h)+} + hH_3O^+ \quad (2.1)$$

$$[M(\underline{OH})(OH_2)_{N-1}]^{(z-1)+} + H_2O \rightarrow [M\underline{O}(OH_2)_{N-1}]^{(z-h)+} + H_3O^+ \quad (2.2)$$

$$Ti(OR)_z + H_2O \rightarrow Ti(OH)(OR)_{z-1} + ROH \quad (2.3)$$

The polymerization begins by binding the OH group to the alkocyte or metal salt. During the condensation reactions 'ol bridge' is formed first.. Hydroxo ligand (OH) is taken between two metals (Pierre, 1998). For example,

$$H_2O\text{-M-} \rightarrow \text{-M-}+H_2O \quad (2.4)$$

$$\text{-M-OH+ -M-} \rightarrow \text{-M-OH-M} \quad (2.5)$$

$$\text{M-OH+-M-OH} \rightarrow \text{-M-OH-M-OH} \quad (2.6)$$

The hydrolysis and condensation reactions proceed together and the reaction rates increase with temperature. (Pierre, 1998).

The structures formed as a result of the processes are solid nanoparticles. These structures occur after the following stages:

Hydrolysis - Condensation - Nucleation - Growth

The gel has a three-dimensional system. It is also permeable (Pierre, 1998). An important criterion for gel formation is the bonding between the smallest solvent particles and the soluble particles. If liquid bonds are made of colloidal left particles, the gel is called colloidal. The molecules that form the gel are bonded to each other by weak or strong bonds to form skeletal tissues with fluid in the spaces between them. Thus, the fluid bonds combine to form the non aqueous gel (Napper & Netschey, 1971).

Wet gel is obtained after geleation occurs. The form of the wet gel changes as long as it is stored in the liquid, this process is called aging. Figure 2.13 shows the appearance of the gels of different structures as a result of aging processes at different temperatures (Pierre, 1998).

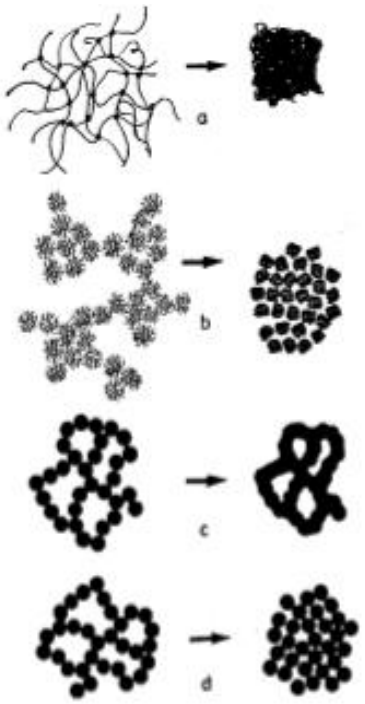


Figure 2.13 Aging process of (a) polymeric gel, (b-c-d) colloidal gel at different temperatures (Pierre, 1998)

Gels show more chemical reactivity than porous solids or powders, thus having catalytic properties (Pierre, 1998).

After the gel has dried, it is usually processed at a temperature much higher than the drying temperature. The reason for this process is to obtain a more robust structure. Often times, there is a chemical change first, each gel has no chemical properties in the desired ceramic. Heat treatment is carried out according to the desired crystal structure. Figure 2.14 shows the changes in the lattice structure by applying calcination (Pierre, 1998).

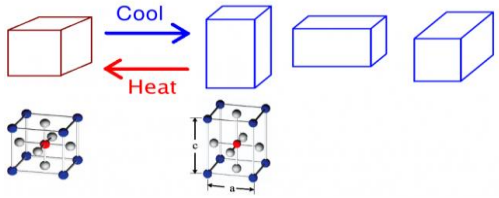


Figure 2.14 Calculation of cage structure as a result of calcination process (Pierre, 1998)

Temperatures vary according to the gel structure, but usually change between 100-300 degrees in crystal structure. According to the temperature values, the organics begin to fly.

1) Solvent or water separation (100$^{o}$C – 150$^{o}$C)

2) Carbon separation (250$^{o}$C – 350$^{o}$C)

3) Oxidation or crystallization (400$^{o}$C – 550$^{o}$C) (Pierre, 1998).

# CHAPTER THREE
# PHOTOCATALYTIC PROPERTIES OF NANOPARTICLES

## 3.1 Photocatalytic Mechanism

The photocatalyst is a semiconductor material that forms a strong oxidizing medium on the surface under the influence of ultraviolet (UV) light. When it is presented to UV light it absorbs the light and converts it into a high energy state and transfers the energy to the surrounding reagents and initiates the chemical reaction. It oxidizes some harmful substances such as germs and mold, which are in contact with the high oxidizing power it produces, and converts it into carbon dioxide, water and other small molecules. Photocatalytic reaction; it is widely utilized in various practises such as smell removal, self-sensing of material and antibacterial (Fujishima, Rao & Tryk, 2000).

The principle capacity of photocatalysis is to expand the speed of the response by diminishing the initiation vitality. Ceramic nanoparticles, such as aluminum oxide $Al_2O_3$, amorphous silica $SiO_2$, magnetite $Fe_3O_4$, titanium dioxide $TiO_2$, zirconium oxide $ZrO_2$ are synthesized to improve specific properties of materials. These nanoparticles have good properties in terms of reactivity and efficiency. Therefore, many studies have been conducted in recent years for the use of these nanoparticles in photocatalytic applications. The main nanoparticles with photocatalytic properties are known as $TiO_2$, ZnO, $SiO_2$ (Paleaz et al., 2012).

Semiconductor materials are characterized by their electronic structures, which are described by "band theory". Band theory, defines all materials as a function of electronic energy levels, called "band". The materials are classified by the energy gap between these bands. While the valance band and the conduction band are adjacent to each other in conductor materials, the non-conductor materials have a very large energy difference between the two bands.

In semiconductors, this band is less than the non-conductors. Owing to external factors, the electrons allow the transition from VB to CB. Such substances which enable the electron to pass from one band to the other are called "photocatalyst" (Sayılkan, 2007). Figure 3.1 shows the non-conductor, semiconductor and conductor band energy levels.

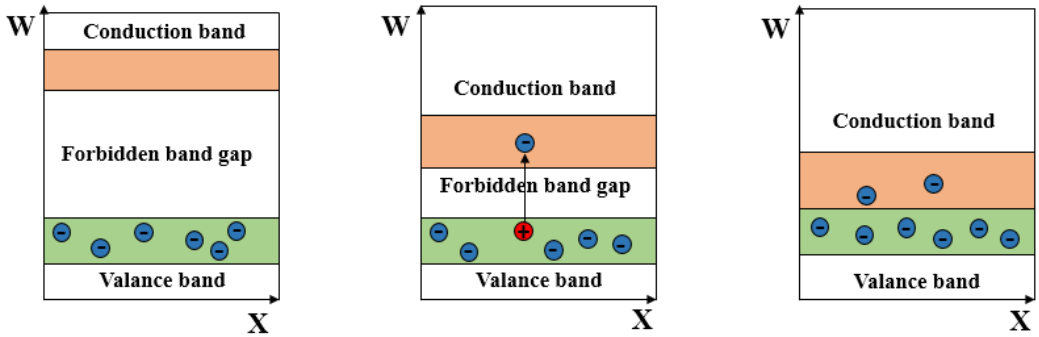


Figure 3.1 Non-conductor, semiconductor and conductor band energy levels

According to the band theory, valence band; energy level filled with electrons that can be excited by external effect, conductivity band; electrons are the energy level remaining empty until they are stimulated. Forbidden band gap shown in Figure 3.1; band energy is the energy level in the middle of the range. This energy level varies according to the type and concentration of any additive added during the synthesis of the semiconductor. Depending on the type of additive added (usually transition metal ion and a small amount of nonmetals), the semiconductor can be produced by controlling the energy range (Sayılkan, 2007).

### 3.2 Factors Affecting Photocatalytic Properties

Photocatalytic activity is defined as the relative or precise speed of the photocatalytic reaction. Photocatalytic efficiency of a catalyst; the surface area and particle size of the semiconductor are influenced by a number of factors. These factors; the crystal size and type of crystal, the type of metal ion added, the applied radiation intensity and irradiation time, ambient temperature, dye concentration in solution, anions and cations in the environment and pH. Almost all of these factors are closely related to the absorbed amount of light sent to the catalyst surface and the scarcity or excess of active places on the catalyst surface (Sayılkan, 2007).

In semiconductors with small particle size, the conductivity band energy level reaches a value bigger than normal, while the VB level remains unchanged. Therefore, as the particle size increases, the semiconductor may be absorbed to a small proportion of the light falling over it, since the band gap energy will also be larger. Therefore, the large particle size reduces the photocatalytic activity of the semiconductor (Almquist & Biswas, 2002).

For the purpose of increased photocatalytic properties of the material many techniques were developed such as surface and chemical modification. For example, metal and nonmetal ion addition occurs when the semiconductor with photocatalytic activity comes into contact with another phase, there is a charge distribution in the semiconductor, which is chemical modification. During the transfer of moving load carriers the electronic band potential of the semiconductor may deteriorate due to the deposition and depletion of the load in areas close to the surface. The added metal and nonmetal concentration is a significant point to enhance photocatalytic activity. One of the biggest advantages of adding metal or ion to the appropriate concentrations is that the semiconductor emits the light absorption spectrum from the ultraviolet region to a wide range of visible regions (> 400 nm) (Sayılkan, 2007).

Lee et al., synthesized Ag single doped $TiO_2$ nanoparticles by sol-gel. They investigated the photocatalytic performance of undoped and Ag single doped $TiO_2$ nanoparticles. They reported that the photocatalytic properties of Ag single doped nanoparticles increased compared to undoped $TiO_2$ (Lee et al., 2005). In another study, Hang et al. undoped and Cr doped $TiO_2$ photocatalyst slim layer were prepared by sol-gel method. The results show that all films have anatase structures and their crystal size is about 18 nm. $TiO_2$ film with 5% Cr added showed the highest photocatalytic efficiency. Cr doped $TiO_2$ slim layers had better photocatalytic activity than undoped $TiO_2$ films under visible light (Hang et al., 2012).

Zhao et al, undoped and Mn/N codoped $TiO_2$ nanoparticles researched the phase form, compound states. They observed that the photoactivity of Mn/N codoped $TiO_2$

was three times greater than that of undoped $TiO_2$ under visible light (Zhao et al., 2016).

### 3.3 $TiO_2$ as Catalyst

$TiO_2$ is a semiconductor activated under UV light. Fujishima and Honda founded that $TiO_2$ was active in the UV region by means of electrodes in 1972 (Fujishima & Honda, 1972). $TiO_2$ can be activated by reactions to change photocatalytic properties. $TiO_2$ in the UV region (280 - 400 nm) is active because of the band gap. $TiO_2$ has a band gap of 3.2 eV. For example, when under UV light irradiation the $TiO_2$ as a catalyst, place a role in optaining OH and O radicals. Theese radicals participate in photocatalytic reactions (Hattori & Tada, 2001).

$TiO_2$ can exist in three different phase form. These are anatase, rutile and brookite. Among these, the best responsive phase to photocatalytic reactions is anatase. Because the electron scattering and adsorption rate in the anatase phase is better than other phases. It can therefore have many uses in the environmental field (Pelaez et al., 2012). The crystallographic properties are shown in Table 3.1.

Table 3.1 Properties of $TiO_2$

| Phase form | Anatase | Rutile |
|---|---|---|
| Bulk density ($g/cm^3$) | 3.89 | 4.25 |
| Melting temperature | 5–6 | 6–7 |
| Crystal structure | Tetragonal | Tetragonal |
| Band gap (eV) | 3.2 | 3.0 |
| Absorbed wavelength beam (nm) | 388 | 413 |

# CHAPTER FOUR
# EXPERIMENTAL STUDIES

In this study, undoped, Cr doped and Cr/N codoped $TiO_2$ nanoparticles were synthesized by sol-gel technique. Cr content was kept constant and N content was altered in order to investigate codoping effect on the photocatalytic properties of nanoparticles.

## 4.1 Synthesis of Nanoparticles

Undoped $TiO_2$, Cr doped $TiO_2$ and Cr-N codoped $TiO_2$ nanoparticles were synthesized by sol-gel tecnique. Titanium tetra-isopropoxide [$Ti(OC_3H_7)_4$] was used as a precursor. Chromium nitrate nanohydrate ($Cr(NO_3)_3 \cdot 9H_2O$) and urea ($NH_2CONH_2$) were used for the Cr and N precursors respectively.

### *4.1.1 Synthesis of $TiO_2$ Nanoparticles*

Titanium (IV) isopropoxide [$Ti(OC_3H_7)_4$], citric acid [$C_6H_8O_7.H_2O$] and deionized water were used as precursors for synthesis of $TiO_2$ nanoparticles. $TiO_2$ sol was prepared by stirring at room temperature titanium tetra-isopropoxide and deionized water with them molar ratio of 1:220. Citric acid solution is then added dropwise to the titanium solution to adjust the pH. The solution is then stirred repeatedly until it has a clear appearance. The solution allowed to dry at 100 ° C and final product was obtained after calcination process that was carried out at 550ºC for about 80 min with a heating rate of about 10ºC per minute in a furnace.

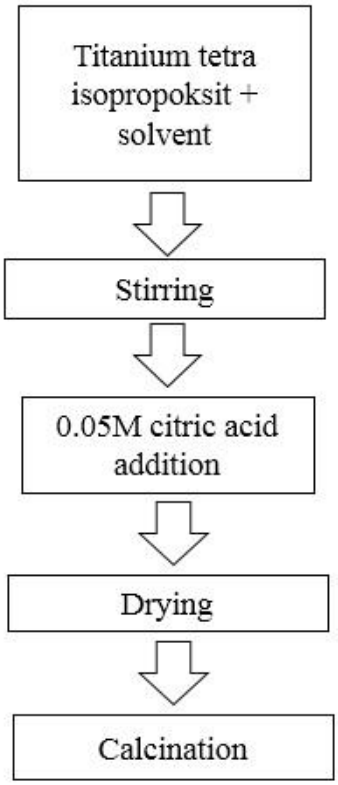


Figure 4.1 The flowchart of the synthesis undoped $TiO_2$ nanoparticles

### *4.1.2 Synthesis of Cr Doped $TiO_2$ Nanoparticles*

Titanium (IV) isopropoxide [Ti(OC3H7)4], chromium (Cr(NO3)3·9H2O) and deionized water were used as precursors for sol-gel synthesis of Cr doped $TiO_2$ nanoparticles. For the synthesis of Cr doped $TiO_2$ nanoparticles, [Ti(OC3H7)4] and deionized water were mixed with 1:220 molar ratio. The solution was magnetically stirred for 30 minutes. Subsequently, 0.125 mol% Cr and deionized water were mixed. This solution added dropwise to titania solution. The solution was left to dry at 100 °C for 43 hours. The obtained gel calcined at 550 °C for 80 min. The flow chart of the synthesis of Cr doped $TiO_2$ nanoparticles by sol-gel tecnique is given in Figure 4.2.

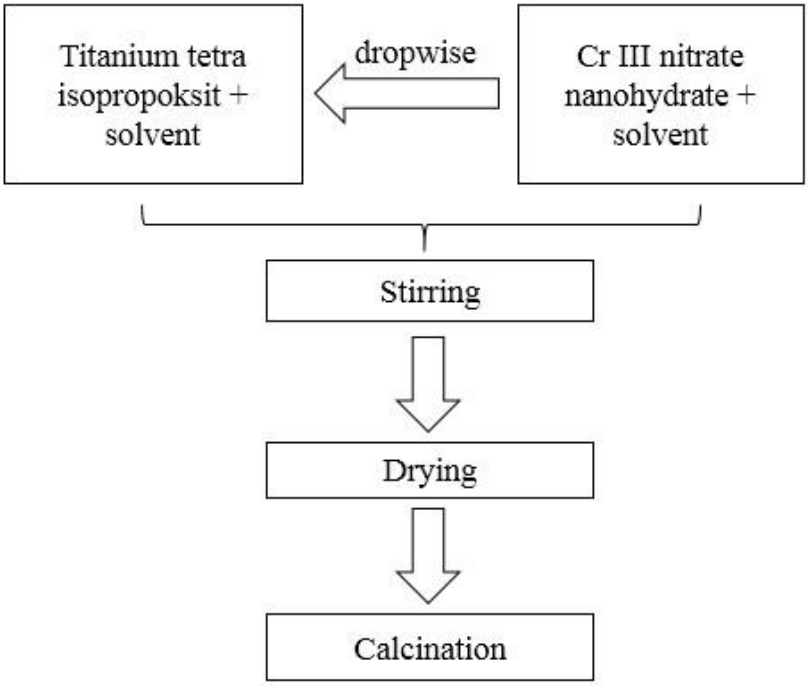


Figure 4.2 Schematic representation of Cr doped $TiO_2$ nanoparticle production

### *4.1.3 Synthesis of Cr-N Codoped $TiO_2$ Nanoparticles*

Titanium (IV) isopropoxide [$Ti(OC_3H_7)_4$], chromium ($Cr(NO_3)_3 \cdot 9H_2O$), urea ($NH_2CONH_2$) and deionized water were used as precursors for sol-gel synthesis of Cr-N codoped $TiO_2$ nanoparticles. For the synthesis of Cr/N codoped $TiO_2$, a precursor solution was prepared by stirring 0.1M [$Ti(OC_3H_7)_4$] with deionized water. Subsequently, 0.125 mol% Cr and deionized water were mixed. Then Cr solution is then added dropwise to the titania solution. This solution is called A solution.

Another solution with 0.1M [$Ti(OC_3H_7)_4$], deionized water and urea ($NH_2CONH_2$) (with different dopant concentration of 0.25%, 0.5% and 1% N) was prepared. Then urea solution was added dropwise to this solution, which is called B solution. The B solution is transferred dropwise to A solution (NH2CONH2) under magnetic stirring. Afterwards, the solution has been dried. Finally, nanoparticles were obtained by calcined at 550°C.

The production of Cr/N codoped $TiO_2$ nanoparticles is given in the Figure 4.3.

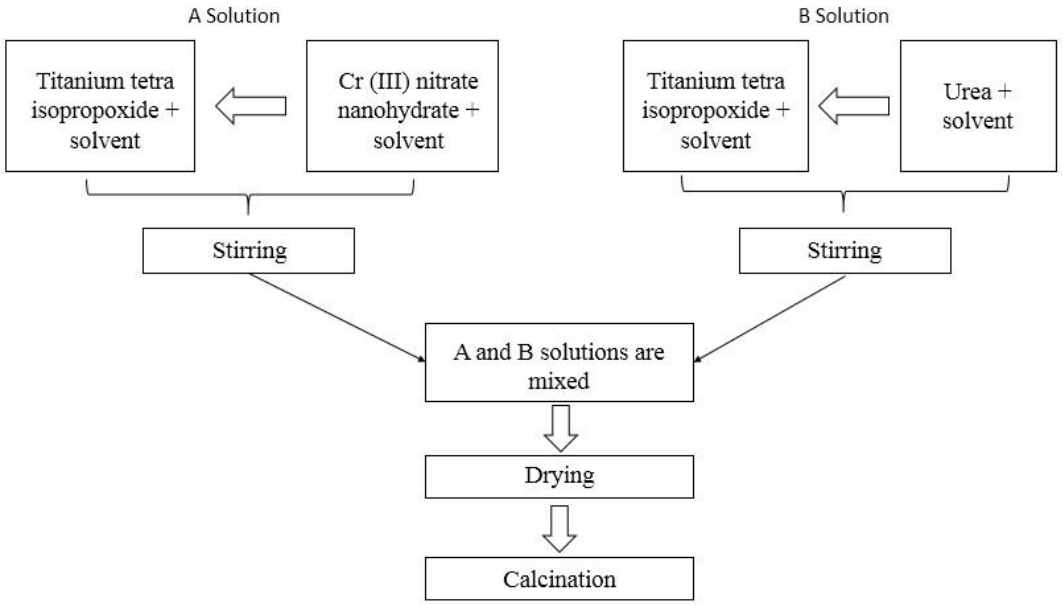


Figure 4.3 The production of Cr/N codoped $TiO_2$ nanoparticles by sol-gel technique

Undoped, Cr doped and Cr/N co-doped $TiO_2$ nanoparticles were named T, TC, TCN1, TCN2 and TCN3 respectively. The properties of the particles are given in Table 4.1.

Table 4.1 Abbreviations of synthesized undoped, Cr doped and Cr/N co-doped $TiO_2$ nanoparticles.

| ***Abbreviation of Nanoparticles*** | ***Cr content (mol%)*** | ***N content (mol%)*** |
|---|---|---|
| T | - | - |
| TC | 0.125 | - |
| TCN1 | 0.125 | 0.25 |
| TCN2 | 0.125 | 0.50 |
| TCN3 | 0.125 | 1 |

## 4.2 Characterization of the Nanoparticles

### *4.2.1 X-Ray Diffraction (XRD)*

The X-Ray Diffraction method (XRD) is based on the fact that each crystalline phase breaks X-rays in a characteristic order, depending on the specific atomic sequences of the phase. For each crystalline phase, these diffraction profiles define that crystal as a kind of fingerprint. The X-Ray Diffraction analysis method does not destroy the sample during the analysis and allows the analysis of even a small amount of samples (Moore & Reynolds, 1997).

The all XRD results were calculated by X-Ray Diffractometer (XRD, Rigaku, D/Max- 2200/PC) with a grazing incident angle of 1° at 40 kV and 36 mA using Cu Kα radiation with a scanning speed of 4° 2θ/min. X-rays strike the sample, causing scattering of atoms. Thus, diffraction patterns of the sample were obtained. As a result of examining the diffraction patterns and comparing the composition with certain standard patterns, the crystal structure of the sample was obtained. The angle at which the constructive interference occurs and the d spacings of the crystals (interplanar distances) are measured using Bragg's Law (4.1):

$$n.\lambda=2.d.\sin\theta \tag{4.1}$$

in which n is an integer, λ is the x-ray wavelength, d is the distance between crystal lattice planes, and Θ is the angle between the incidence ray and the scattering plane (degrees). When the X-rays is plotted as a function of the angle, an XRD model which is characteristic for the sample is obtained (Feddes, Gonzalez, Serra, Pou, Chiussi & Wolke, 2009).

### *4.2.2 Particle Size Analyser*

The laser diffraction particle size analyzer includes a laser device as a light source to produce an ultraviolet laser beam. The material is placed in a transparent solution.

It is then placed in the device. The laser beam penetrates the material and the intensity of the refracted light is measured with the help of detectors and reflected on the screen. In this way, the Zetasizer device provides information about the particle size of the material (Instruments, 2004).

In this study, the particle sizes of the nanoparticles were measured by the Malvern Zeta Sizer Nano ZS90.

### *4.2.3 X-ray Photoelectron Spectrometry (XPS) Analysis*

X-ray photoelectron spectroscopy (XPS) is a commonly used the characterization technique for elemental composition and electronic states of the samples. XPS is an analysis method that requires high vacuum and as clean a surface as possible. XPS monitors the binding energies of the elements and analyzes them by measuring scattered electrons (Yang, Bai, Tan & Lian, 2006).

In this study, XPS analysis has been done with K-Alpha X-ray photon spectrophotometer with Al Kα micro-focused monochromator with variable spot size (30-400μm in 5μm steps) source.

### *4.2.4 Fourier Transform Infrared Spectroscopy (FTIR) Analysis*

The FTIR device is able to determine organic matter by using infrared light in the wavelength range of 400-4000 $cm^{-1}$. Percent transmittance (% T), percent absorbance (% A) depends on the percentage of reflectance (% R) in order to obtain the characteristic peaks of the substance. After certain measurement preparations have been completed, the determination of the elemental analysis can be made easily and in a short time (Griffiths, 1983).

In this study, the Fourier Transform Infrared Spectroscopy (FTIR) analysis were conducted with NICOLET iS10 to determine functional groups in nanoparticles. Measurements were conducted with wave number range of 4000–550 $cm^{-1}$. The FTIR

spectrum gives an idea of $TiO_2$, Cr doped $TiO_2$, Cr/N codoped $TiO_2$ surface functional groups.

### *4.2.5 Measurement of photocatalytic activity*

The photocatalytic activity of produced nanoparticles were examined by degradation of methylene blue (MB) under UV light irradiation. 1 mL of methylene blue and 99 mL of deionized water were prepared as an initial concentration. 0.05 g of Cr doped $TiO_2$ or Cr/N codoped nanoparticles were mixed into a 50 mL methylene blue concentration. The solution was centrifuged for 6 minutes to obtain a homogeneous suspension. Afterwards, the suspension is exposed to irradiation under the Osram, UltraVitalux E27, 300W lamp as UV light source. During irradiation, the reaction medium was continuously purged with air at a continuous flow rate to ensure adequate $O_2$ concentration. Samples of 50 ml were collected every 15 min and measured by UV spectroscopy. This process continued for a total of 60 minutes, with a measurement every 15 minutes. After each interval absorbsion of solution was measured by UV-vis spectrophotometer (UV mini-1240, Shimadzu) at a wavelength of 664 nm.

In order to determine residual MB percentage in the solution, degradation rate was calculated with the equation: $((C_0\text{-}C)/C_0) \times 100$, where $C_0$ and C are the initial concentration value of MB and the concentration value after irradiation, respectively (Koh, Hatta, Ong, Yuliati & Lee, 2017).

# CHAPTER FIVE
# RESULTS AND DISCUSSION

## 5.1 Characterization of Synthesized Nanoparticles

XRD analysis of synthesized nanoparticles were done with Rigaku D/Max-2200/PC X-ray diffractometer with Cu Kα radiation ( $\lambda$ = 0.1542 nm) at 40 kV and 30 mA over $2\theta$ range of 3–$90^0$, in order to determine crystal structure and crystal size. Figure 6.1 shows, all nanoparticles composed of anatase peaks at 2θ = 25.2°, 37.8°, 48.05°, 53.8°, 55.06°,62.9°, 68.7° 70.3°, 75.03° and 82.6°. These peaks correspond to the reflections from (101), (004), (200), (105), (211), (204), (116), (107) and (303) planes of the crystal lattice (Anatase XRD JCPDS Ref. No. 21-1272). The ions and dimensions of the additive element can affect the $TiO_2$ lattice structure and cause changes. The Cr ions used in the synthesis are similar in structure to Ti ions ($Cr^{3+}$ ionic radius = 0.615, $Ti^{4+}$ ionic radius = 0.605). Therefore, $Ti^{4+}$ and $Cr^{3+}$ ion exchange is possible (Koh et al., 2017).

Particle size analysis of undoped, Cr doped and Cr/N codoped $TiO_2$ nanoparticles are given in Table 5.1 (Quan et al., 2014).

Table 5.1 Particle size values of synthesized nanoparticles

| ***Sample*** | ***Particle Size (nm)*** |
|---|---|
| T | 68.70 |
| TC | 75.80 |
| TCN1 | 86.12 |
| TCN2 | 70.35 |
| TCN3 | 67.03 |

According to XRD results, doping Cr and N to the $TiO_2$ crystal structure did not change the crystal structure of $TiO_2$. Peak broadening has been observed due to Cr and

N contribution to $TiO_2$ structure (Kurtoglu, Longenbach, Sohlberg & Gogotsi, 2011). Koh et al. studied on contribution of different consantration Cr in $TiO_2$ structure. It was observed that the Cr doping did not cause a change in the crystal structure of $TiO_2$. They also reported that the intensity of diffraction peaks increased with increasing Cr contribution (Koh et al., 2017).

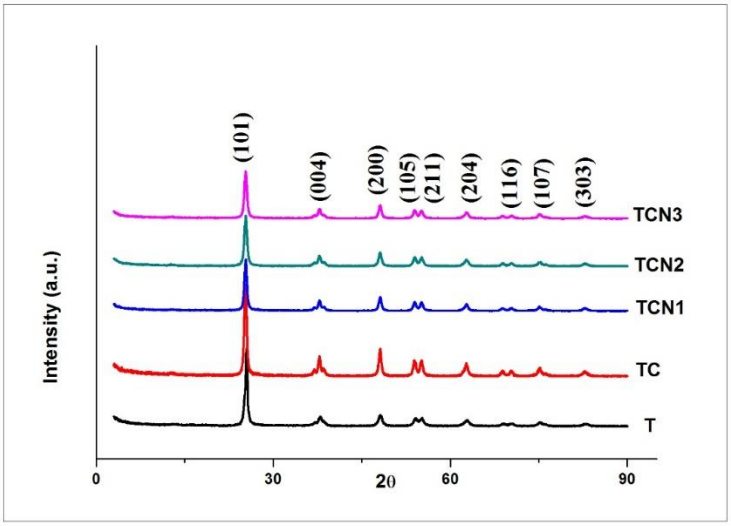


Figure 5.1 X-Ray Diffraction (XRD) patterns of the undoped, Cr doped and Cr/N codoped $TiO_2$ nanoparticles

The particle sizes of the nanoparticles were measured by the Malvern Zeta Sizer Nano ZS90. The results of particle size analysis of undoped, Cr doped and Cr/N codoped $TiO_2$ nanoparticles are given in Figure 5.2. The size of the nanoparticles was calculated as ~ 70 nm for Cr doped and Cr/N codoped $TiO_2$ nanoparticles. The particle size results shows that doping process restricted the crystal size growth. Also a reduction in particle size was observed. TCN3 nanoparticles were measured as the smallest size nanoparticles (67.03 nm).

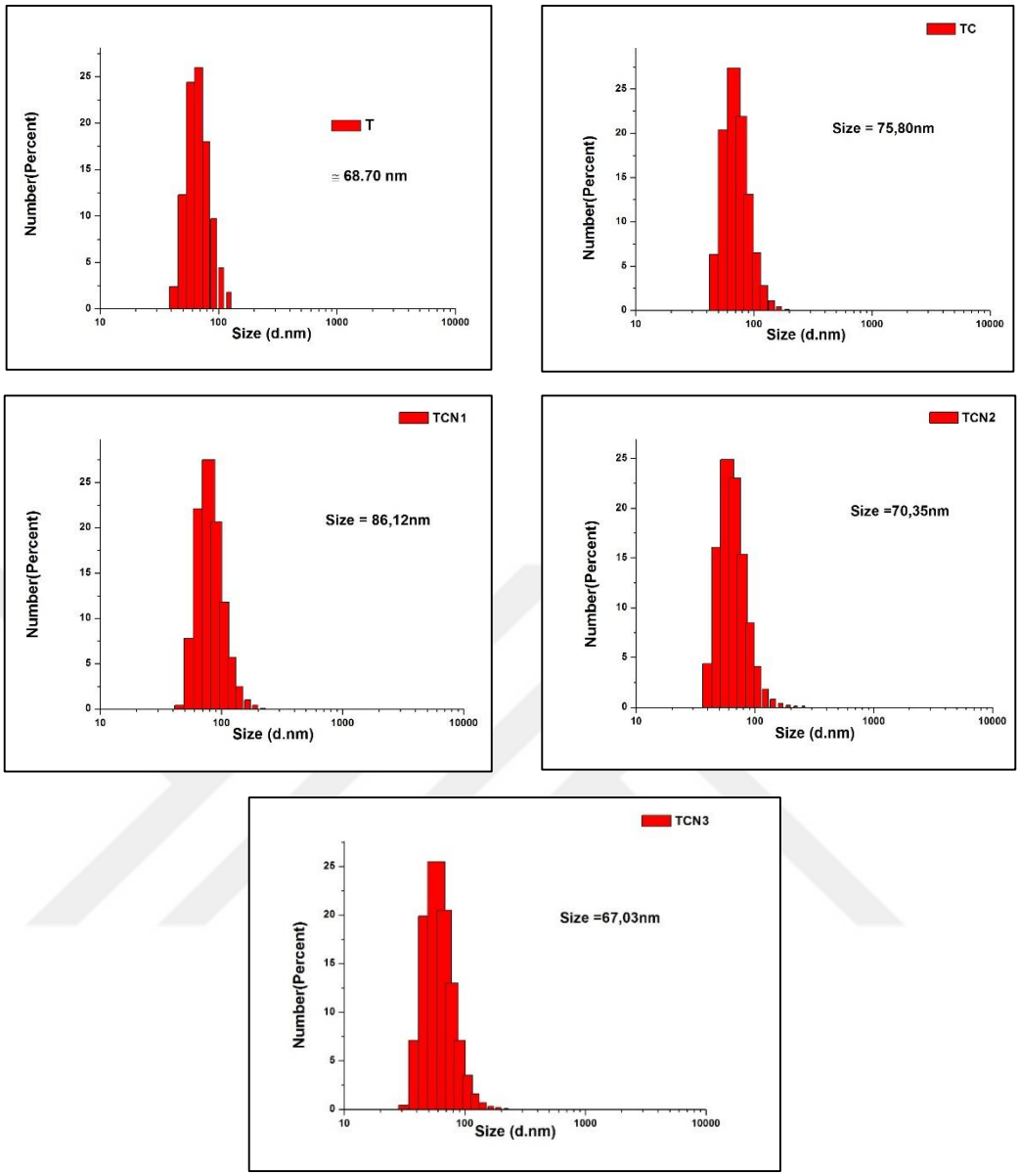


Figure 5.2. Particle size graphs of T, TC, TCN1, TCN2, TCN3 nanoparticles

XPS analysis has been done with K-Alpha X-ray photon spectrophotometer with Al Kα micro-focused monochromator with variable spot size (30-400µm in 5µm steps) source in order to determine electronic state and nanoparticle composition.

XPS measurement of synthesized nanoparticles was carried out to demonstrate Cr doping and Cr/N codoping into $TiO_2$ structure depicted in Figure 5.3(a-f). The global spectra of undodped, Cr doped and Cr/N codoped nanoparticles shows characteristic split signal corresponding to the Ti2p of $Ti^{4+}$ state in $TiO_2$ (Figure 5.3(a)), as well as the Cr 2p, N 1s and O 1s signals. Since XPS analysis conducted with carbon tape, the

main spectrum shows C 1s peak at 284.6 eV. The O 1s peak located at 529.57 eV. The Cr 2p region observed between at 594 and 572.47 eV. The N 1s peak located approximately at 400 eV.

Figure 5.3 (b) depicts charcateristic peaks of Ti2p3/2 and Ti2p1/2 located at 458.37 eV and 464.39 eV, respectively. The results show that the binding energy of Ti ions can be further reduced by the addition of Cr ions and N ions (Chen & Burda, 2004).

Figure 5.3 (c) shows the XPS spectrum of the O1s region. The main peaks of O1s are located near 529.57 eV. The Cr2p region observed in Figure 5.3 (d) is between 594 and 572.47 eV. This result is consistent with reported XPS results using chrome as a dopant. Cr/N codoped $TiO_2$ nanoparticles are shifted to lower binding energies at Cr2p levels than Cr doped $TiO_2$ (Kurtoglu et al., 2011).

There is characteristic N1s peak with low binding energy approximately at 400 eV as shown in Figure 5.3 (e), suggesting that nitrogen succesfully incorporated to the $TiO_2$ structure, which can be observed at 404.76 and 394.90 eV (Nakamura, Tanaka & Nakato, 2004).

Figue 5.3 (f) shows Ti 2p states of undoped, chromium doped and co-doped $TiO_2$ nanoparticles. The Ti2p3/2 and Ti2p1/2 charcateristic peaks of undoped $TiO_2$ located at 459.25 eV and 467.12 eV. The Ti2p region of the N / Cr co-doped $TiO_2$ is between 458.37 and 464.39 eV. Compared to the undoped nanoparticles it can be seen that there is decrease in binding energy. The shift in binding energy indicates that substitution of chromium and nitrogen atoms were successfull (Yuan, Jia & Zhang, 2002).

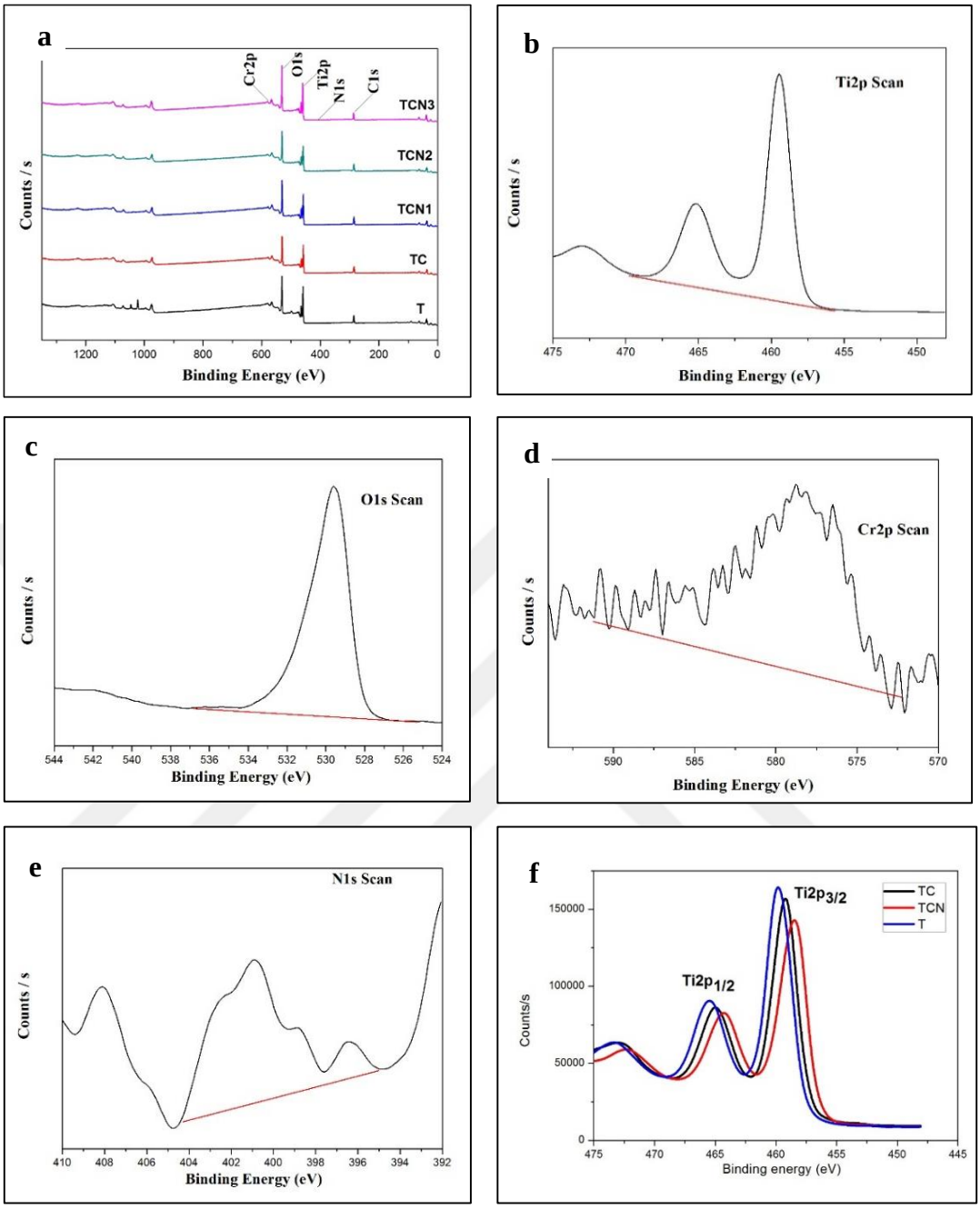


Figure 5.3. XPS spectra of the nanoparticles around (a) Global XPS spectra of undoped, Cr doped and Cr/N codoped $TiO_2$ nanoparticles, (b) Ti 2p characteristic peaks of Cr/N codoped $TiO_2$ nanoparticles, (c) O 1s characteristic peaks of Cr/N codoped $TiO_2$ nanoparticles, (d) Cr 2p characteristic peaks of Cr/N codoped $TiO_2$ nanoparticles and (e) N 1s characteristic peaks of Cr/N codoped $TiO_2$ nanoparticles (f) Ti 2p characteristic peaks of undoped, Cr doped, Cr/N codoped $TiO_2$ nanoparticles

FTIR analysis were conducted with NICOLET iS10 to determine functional groups in nanoparticles. Measurements were conducted with wave number range of 4000–550 $cm^{-1}$. The FTIR spectrum gives an idea of undoped $TiO_2$, Cr doped $TiO_2$, Cr/N

codoped $TiO_2$ surface functional groups. The FTIR spectra of all synthesized nanoparticles are shown in the Figure 5.4. The main absorption peaks were located at 2350, 1596, 1465, 820 $cm^{-1}$ in all five samples.

The bands between 3417 and 3000 $cm^{-1}$ are due to hydroxyl stretching vibration bands (Leon, Reuquen, Garin & Segura, 2017). Also the O-H band was observed at the peak at 1610 $cm^{-1}$ (Senthilnathan & Philip, 2010). The peaks at 2350 $cm^{-1}$ and 1465 $cm^{-1}$ corresponds to C-H bonds. The absorption band between 1000-600$cm^{-1}$ indicates the O-Ti-O stretch region (Khairy & Zakaria, 2014). The peak at 1350 $cm^{-1}$ is resulted from nitrogen doping. As the concentration of N increased, the peak intensity has increased (Xu et al., 2008). The peak at 1210$cm^{-1}$ is a new peak due to Cr doping. Theese peaks indicates the successful doping of the Cr and N additives. No organic residue was found in any of the samples (Senthilnathan & Philip, 2010).

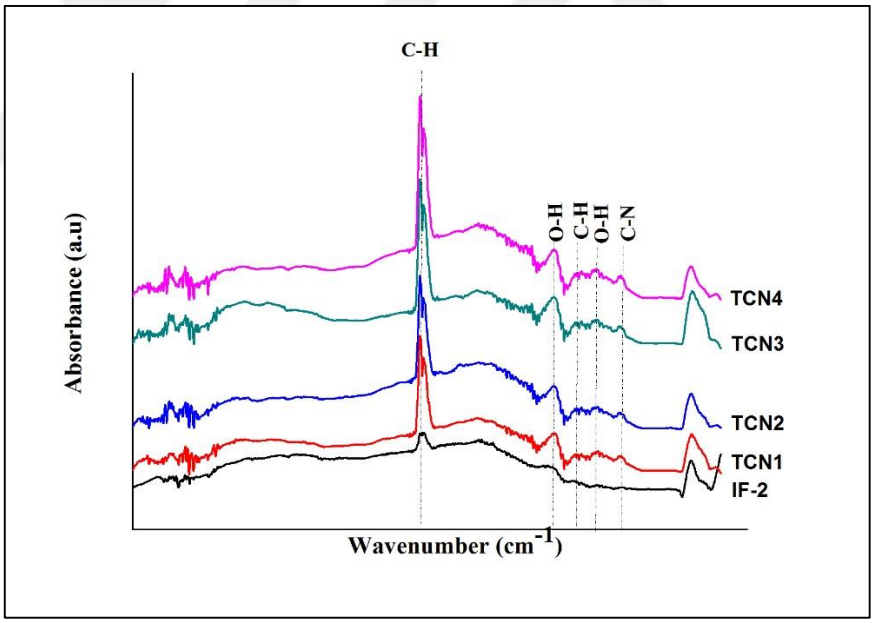


Figure 5.4 FTIR spectra of undoped, Cr doped and Cr/N codoped $TiO_2$ nanoparticles

## 5.2 Photocatalytic Properties of Synthesized Nanoparticles

$TiO_2$ is activated under UV irradiation and photocatalytic reactions begin to occur. As the electrons pass from the VB to the CB, it creates a positively charged hole. They also cause chemical reactions between the donor (D) and acceptor (A) components

(5.2 – 5.3). This results in a load balance (Kumar & Devi, 2011; Fujishima, Rao & Tryk, 2000):

$$D + h^+ \rightarrow D^+ \quad (5.2)$$

$$A + e^- \rightarrow A^- \quad (5.3)$$

The holes formed by excited electrons on the valence band have oxidation properties. When the UV light energy excess the energy of $TiO_2$ nanoparticle, an electron from Ti is excited from VB to CB (5.4). Excited electrons react with water to form hydroxyl radicals (OH•) and superoxide ions ($O_2^-$). These reactions may occur due to the oxidizing properties of $TiO_2$ (5.5 - 5.7). These radical ions formed can easily react with organic compounds. Oxidation properties are very high. The photocatalytic reactions in MB solution are given in equations below:

$$Ti^{5+} + h^+ \rightarrow Ti^{4+} \quad (5.4)$$

$$H_2O + h^+ \rightarrow OH + h^+ \quad (5.5)$$

$$O_2^+ + e^- \rightarrow O_2^- \quad (5.6)$$

$$Ti^{4+} + O_2 \rightarrow Ti^{5+} + O_2\bullet \quad (5.7)$$

$Cr^{3+}$ ions prevented the formation of recombination during reactions with $Cr^{4+}$ ions and caused the formation of radical ions. (Koh et al., 2017). In additon the Cr atoms have similar reactions to Ti, considering that it is also transition metal, which is given in equations below (5.5 – 5.12):

$$Cr^{3+} + h^+ \rightarrow Cr^{4+} \quad (5.8)$$

$$H_2O + h^+ \rightarrow OH + h^+ \quad (5.9)$$

$$Cr^{4+} + OH^- \rightarrow Cr^{3+} + OH\bullet \quad (5.10)$$

$$O_2^+ + e^- \rightarrow O_2^- \quad (5.11)$$

$$Cr^{3+} + O_2 \rightarrow Cr4+ + O_2^- \quad (5.12)$$

The doping of nonmetals has resulted in contracting of band gap. The role of nitrogen atoms is to contract band gap of $TiO_2$, which makes excitations of electrons easier. Thus, the utilization efficiency of visible light is increased (Lee et al., 2005).

Photocatalytic efficiency of undoped an doped nanoparticles were determined based on the rate of degradation of MB (methylene blue). Figure 5.5 shows absorbance spectrums of all nanoparticles with 15 minute intervals. 1% Cr/N codoped $TiO_2$ nanoparticles were calculated as nanoparticles having the best photocatalytic efficiency under UV light. An enhance in photocatalytic activity was observed with the contribution of N (Li, Jiang, Peng & Jiang, 2010).

If the content of Cr is relatively low, Cr can to play a role as a charge trap affecting the recombination rate. The surface area of Cr/N codoped $TiO_2$ with 0.125% Cr and 1% N doping concentration is larger than the other nanoparticles. The large surface area allows for a smaller particle size and increased photocatalytic efficiency.

Figure 5.6 shows the absorbance values of MB degradation of undoped, Cr doped and Cr/N codoped $TiO_2$ nanoparticles. The results show that N doping induces a increase of photocatalytic efficiency values from 79.34% to 99.60%.

Figure 5.7 shows the photodegradation efficiency of MB (methylene blue) over undoped $TiO_2$, Cr doped $TiO_2$ and Cr/N codoped $TiO_2$ nanoparticles. All Cr/N codoped $TiO_2$ samples have higher photocatalytic activity than Cr doped $TiO_2$. The best photoactivity is observed in the TCN3 (1% Cr/N codoped $TiO_2$) sample. The photocatalytic efficiency of undoped $TiO_2$, 0.125% Cr doped $TiO_2$, 0.25% Cr/N codoped $TiO_2$, 0.5% Cr/N codoped $TiO_2$ and 1% Cr/N codoped $TiO_2$ samples were 79.34%, 90.47% 84.47%, 92.69%, 99.60%, respectively.

Cr and N codoped nanoparticles showed higher photocatalytic efficiency than TC nanoparticles. The Cr / N codoping process increased the amount of electron scattering to ensure load balance and thus increased photocatalytic efficiency.

Cr and N codoped $TiO_2$ nanoparticles have a lower crystal size and particle size than Cr and undoped $TiO_2$ nanoparticles. This shows that particle size and crystal size are well affected when codoping to the structure of the semiconductor materials. Thus, the surface area of the nanoparticles is increased and optical absorption is improved. N dopant atoms constrict the band gap and facilitated the scattering of electrons. Recombination formation was prevented and photocatalytic efficiency increased (Quan et al., 2014).

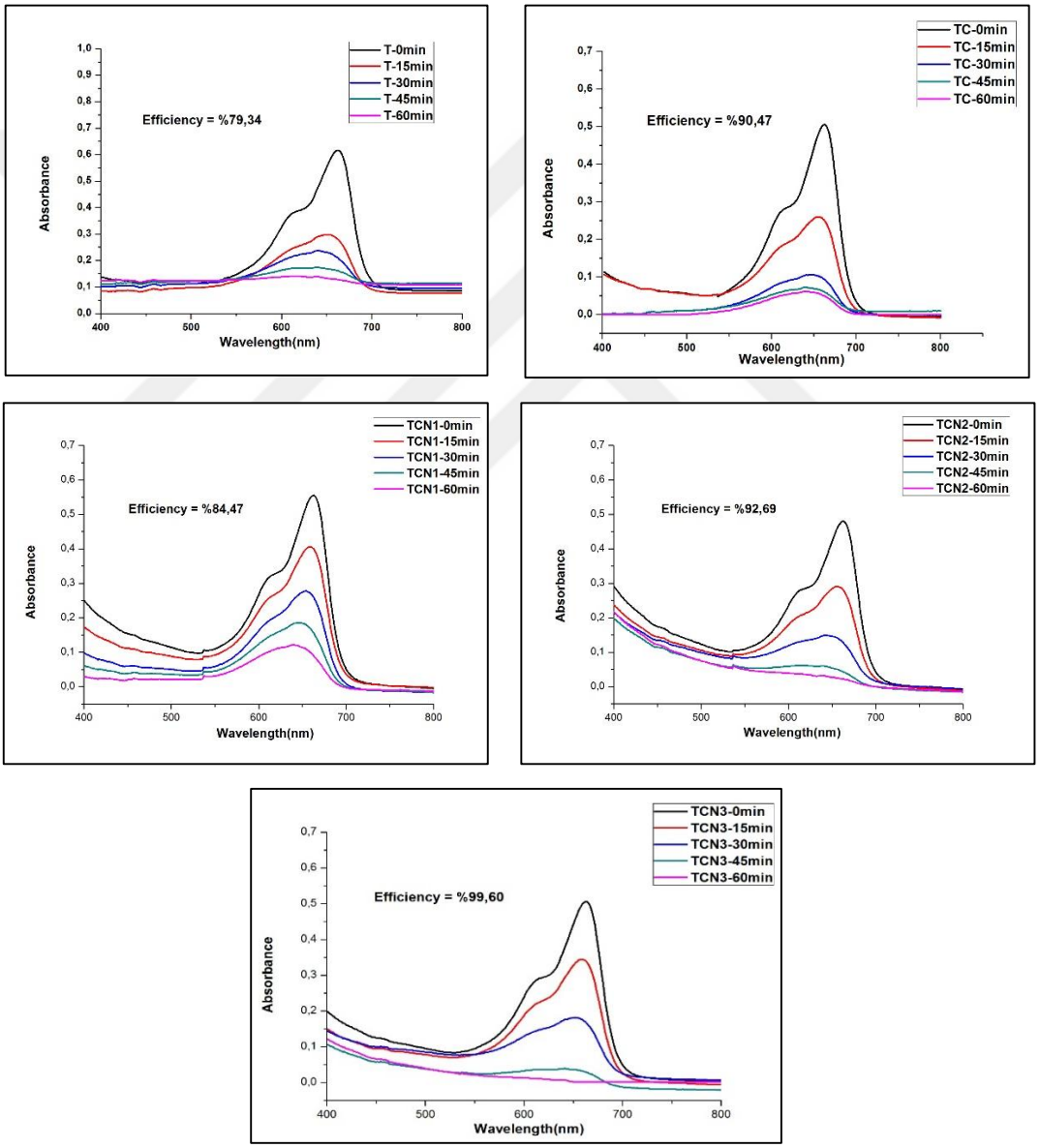


Figure 5.5 Photocatalytic activity results of T, TC, TCN1, TCN2, TCN3 nanoparticles

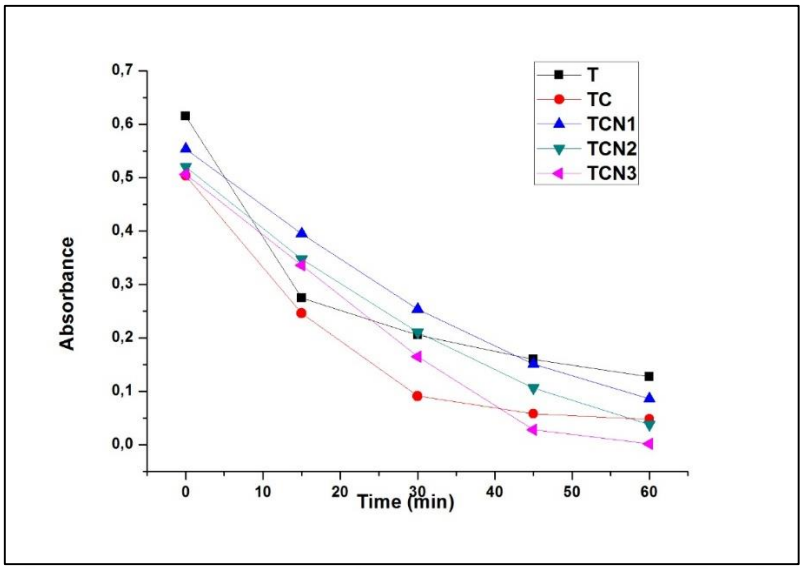


Figure 5.6 Spectra of Methylene Blue degradation under solar irradiation of T, TC, TCN1, TCN2, T

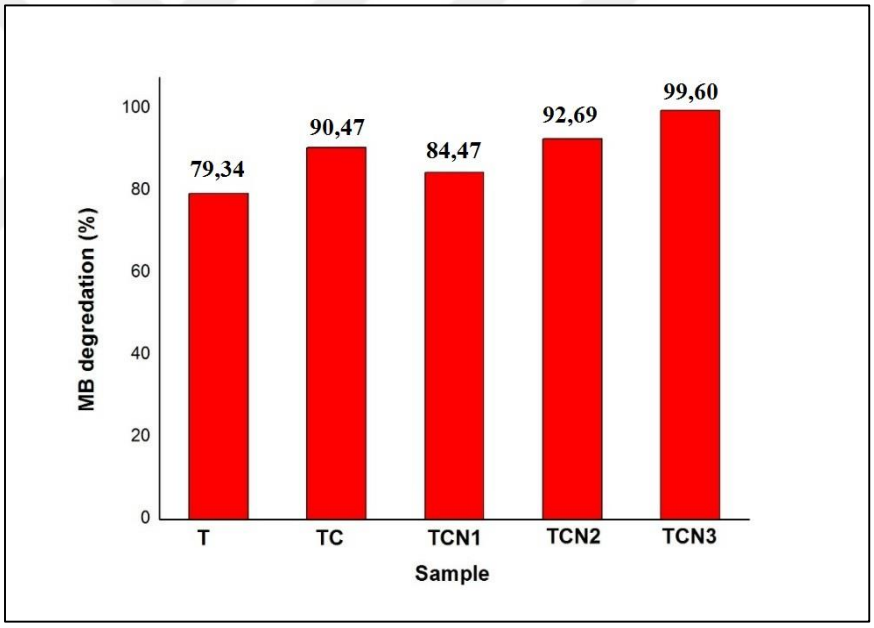


Figure 5.7 Photodegradation efficiency of MB (methylene blue) over undoped $TiO_2$, Cr doped $TiO_2$ and Cr/N codoped $TiO_2$ nanoparticles under visible light irradiation for 60 min

# CHAPTER SIX
# CONCLUSION

In this study, undoped $TiO_2$, Cr doped $TiO_2$ and Cr/N codoped $TiO_2$ nanoparticles were successfully synthesized by sol gel tecnique. The Cr content was kept constant and the N content was modified to investigate how the codoping method affected the photocatalytic properties of the nanoparticles.

The particle sizes of the nanoparticles were measured by the Malvern Zeta Sizer Nano ZS90. Crystalline structure, crystalline size of nanoparticle and elemental additions analysis were conducted with X-ray Diffraction (XRD). Chemical composition and electronic structures were determined with X-ray photoelectron spectrometry (XPS). Surface functional groups of undoped, Cr doped and Cr/N codoped $TiO_2$ were analyzed using FTIR. The photocatalytic efficiency analysis of undoped, Cr doped and Cr/N codoped $TiO_2$ nanoparticles was performed using UV-vis spectrophotometer. Photocatalytic efficiency values were evaluated by measuring degredation of methylene blue under UV-light irridation.

- XRD results show that all synthesized nanoparticles are in the anatase phase. Elemental additives to the $TiO_2$ structure did not affect the crystal structure of synhesized $TiO_2$ nanoparticles.

- The size of the nanoparticles was measured as ~ 70 nm for T, TC, TCN1, TCN2 and TCN3 samples. The particle size of TCN 3 nanoparticles is smaller compared to synhesized other nanoparticles (TCN3 = 67.03nm).

- XPS results show that Cr/N codoped $TiO_2$ nanoparticles are shifted to lower binding energies than Cr doped $TiO_2$ at Ti 2p levels, which indicates the doping was successful.

- According to the analysis results under visible light irradiation, the nanoparticles in which Cr and N elements were added together to the $TiO_2$

structure had more photoactivities compared to single doped Cr and undoped $TiO_2$. In photocatalytic efficiency analyzes, nanoparticles with the highest results are TCN3 nanoparticles. The photocatalytic efficiency of the TCN3 nanoparticles in MB solution were 99.60%. It is observed that the codoping of nonmetal and metal elements provides a photocatalytic efficiency enhancing effect.

## REFERENCES


Al-Salim, N.I., Bagshaw, S.A., Bittar, A., Kemmitt, T., McQuillan, A.J., Millsa, A.M., & Ryan, M. J. (2000). *Journal of Materials Chemistry, 10,* 2358–2363

Alvarez, S. Y. M., Mar, J. L. G., Palomino, G. T., Alejandro, F. M., Ramírez, A. H., & Reyes, L. H. (2017). UV and visible activation of Cr(III)-doped $TiO_2$ catalyst prepared by a microwave-assisted sol–gel method during MCPA degradation. *Environmental Science and Pollution Research, 24,* 12673–12682

Alvarez, S. Y. M., Mar, J. L. G., Palomino, G. T., Alejandro, F. M., Quintero, A. C., Ramírez, A. H., & Reyes, L. H. (2019). Synthesis of $Cr^{3+}$-doped $TiO_2$ nanoparticles: characterization and evaluation of their visible photocatalytic performance and stability. *Environmental Technology, 40,* 144 – 153

Bagheri, S., Shameli, K., & Hamid, S. B. A. (2013). Synthesis and characterization of anatase titanium dioxide nanoparticles using egg white solution via sol-gel method. *Journal of Chemistry, 848205,* 5-10

Bechstein, R., Kitta, M., Schutte, J., Kuhnle, A., & Onishi, H. (2009). *Journal of Physical Chemistry, C 113,* 13199–13203

Bhaviripudi, S., Mile, E., Steiner, S.A., Zare, A.T., Dresselhaus, M.S., Belcher, A.M., & Kong, J. (2007). *Journal of the American Chemical Society, 129* (6), 1516-1517

Buzea, C., Pacheco, I. I., & Robbie, K. (2007). Nanomaterials and nanoparticles: Sources and toxicity. *Biointerphases, 4,* 17-71

Carp, O., Huisman, C.L., & Reller, A. (2004). Photoinduced reactivity of titanium dioxide. *Progress Solid State Chemistry, 32,* (1), 33–177

Chen, X., & Burda, C. (2004). Photoelectron spectroscopic investigation of nitrogen-doped. Titania nanoparticles. *Journal of Physical Chemistry, B 108,* 15446–15449

Choi, W., Termin, A., & Hoffmann, M.R. (1994). The role of metal ion dopants in quantum-sized $TiO_2$: correlation between photoreactivity and charge carrier recombination dynamics. *Journal of Physical Chemistry, 98,* 13669–13679

Cong, Y., Zhang, J., Chen, F., Anpo, M., & He, D. (2007). Preparation, photocatalytic activity and mechanism of nano-$TiO_2$ co-doped with nitrogen and iron (III). *The Journal of Physical Chemistry, 111,* 10618-10623

Dalvandi, M., & Ghasemi, B. (2013). Synthesis of titanium dioxide nano-powder via sol–gel method at ambient temperature. *Journal of Sol-Gel Science and Technology, 66,* 68–72

Dave, P.N., Chaturvedi, S. (2011). A review on nano-$TiO_2$ sol–gel type syntheses and its applications. *Journal of Material Science, 46,* 3669–3686

Deng, Q.R., Xia, X.H., Guo, M.L., Gao, Y., & Shao, Diwald, O., Thompson, T.L., Zubkov, T.E., Goralski, G., Walck, S.D., & Yates, J.T. (2004). Photochemical activity of nitrogen-doped rutile $TiO_2$ in visible light. *The Journal of Physical Chemistry, 108,* 6004–6008

Emeline, A.V., Kuznetsov, V.N., Rybchuk, V.K., & Serpone, N. (2007). Visible-light-active titania photocatalysts: the case of N-doped $TiO_2$ – properties and some fundamental issues. *International Journal of Photoenergy, 19,* 547-562

Feinle, A., Elsaesser, M.S., & Hüsing, N. (2016). Sol–gel synthesis of monolithic materials with hierarchical porosity. *Published in Chemical Society reviews, 20* (8), 54-68

Fujishima, A., & Honda, K. (1972). Photolysis-decomposition of water at the surface of an irradiated semiconductor. *Nature*, *238* (5385), 37–38

Fujishima, A., Rao, T.N., & Tryk, D.A. (2000). $TiO_2$ photocatalysts and diamond electrodes. *Electrochimica Acta, 45*, 4683–4690

Hahn, H. (1997). Gas phase synthesis of nanocrystalline materials. *Nanostructured Materials, 9,* 3-12

Hang, P. N. T., Ke, N. H., Phuong, D. A., & Hung, L. V. T. (2011). Enhancing the photocatalytic activity under visible light of chromium doped $TiO_2$ thin film prepared by sol-gel method. *Journal of Science, Mathermatics – Physics, 27,* 251-257

Hong, I. (2006). VOCs degradation performance of $TiO_2$ aerogel photocatalyst prepared in SCF drying. *Journal of Industrial and Engineering Chemistry, 12* (6), 918–925

Griffiths, P. (1983). Fourier transform infrared spectrometry. *Article in Science, 10,* 75-93

Instruments, M. (2004). *Zetasizer nano series user manual*. Worcester: Malvern Instruments.

Iwasaki, M., Hara, M., Kawada, H., Tada, H., & Ito, S. (1999). Cobalt ion-doped $TiO_2$ photocatalyst response to visible light. *Journal of Colloid and Interface Science, 224*, 202–204.

Jeffrey, C., Wu, S., & Chen, C. (2004). *Journal of Photochemistry and Photobiology A: Chemistry, 163*, 509–515

Jia, Li., Wu, C., Li, Y., Han, S., Li, Z., Chi, B., Pu, J., & Jian, L. (2011). Enhanced visible-light photocatalytic activity of anatase $TiO_2$ through N and S codoping. *Applied Physics Letters, 98,* 211903.

Kakihana, M. (1996). Invited review sol-gel preparation of high temperature superconducting oxides. *Journal of Sol-Gel Science and Technology, 6,* 7-55

Khairy, M., & Zakaria, W. (2014). Effect of metal-doping of $TiO_2$ nanoparticles on their photocatalytic activities toward removal of organic dyes. *Egyptian Journal of Petroleum, 23,* 419–426

Koh, P.W., Hatta, M.H.M., Ong, S.T., Yuliati, L., & Lee, S.L. (2017). Photocatalytic degradation of photosensitizing and non-photosensitizing dyes over chromium doped titania photocatalysts under visible light. *Journal of Photochemistry and Photobiology A: Chemistry, 332,* 215–223

Kurtoglu, M.E., Longenbach, T., Sohlberg, K., & Gogotsi, Y. (2011). Strong coupling of Cr and N in Cr_N-doped $TiO_2$ and its effect on photocatalytic activity. *Journal of Physical Chemistry, 115,* 17392 - 17399

Lee, M., Hong, S., & Mohseni, M. (2005). Synthesis of photocatalytic nanosized $TiO_2$–Ag particles with sol–gel method using reduction agent. *Journal of Molecular Catalysis A: Chemical, 242,* 135–140

Leon, A., Reuquen, P., Garin, C., & Segura, R. (2017). FTIR and Raman characterization of $TiO_2$ nanoparticles coated with polyethylene glycol as carrier for 2-methoxyestradiol. *Applied Sciences, 7* (1), 49

Li, Y., Jiang, Y., Peng, S., & Jiang, F. (2010). Nitrogen-doped $TiO_2$ modified with $NH_4F$ for efficient photocatalytic degradation of formaldehyde under blue light-emitting diodes. *Journal of Hazardous Materials, 182,* 90–96

Li, H., Wang, J., Li, C., Wang, T., & Zhao, Y. F. (2015). Photonic and photocatalytic behavior of $TiO_2$ mediated by Fe, CO, Ni, N doping and co-doping. *Physica, B 478*, 6–11

Mallakpour, S., & Madani, M. (2015). A review of current coupling agents for modification of metal oxide nanoparticles. *Progress in Organic Coatings, 86,* 194–207

Martin, S. T., Morrison, C. L., & Hoffmann, M. R. (1994). Photochemical mechanism of size-quantized vanadium-doped $TiO_2$ particles. *Journal of Physical Chemistry, 98,* 13695-13704

Mills, A., & Le Hunte, S. (1997). An overview of semiconductor photocatalysis. *Journal of Photochemistry and Photobiology A: Chemistry, 108* (1), 1-35

Moore, D. M., & Reynolds, R. C. (1997*). X-Ray Diffraction and the Identification and Analysis of Clay Minerals.* New York: Oxford University Press

Nakamura, R., Tanaka, T., & Nakato, Y. (2004). Mechanism for visible light responses in anodic photocurrents at N-doped $TiO_2$ film electrodes. *Journal of Physical Chemistry, B 108,* 10617–10620

Napper, D.H., & Netschey, A. (1971). Studies of the steric stabilization of colloidal particles. *Journal of the Colloid Interface Science, 37* (3), 528–535

Ovais, M., Raza, A., Naz, S., Islam, N. U., Khalil, A. T., Ali, S., Khan, A. M., & Shinwari, Z. K. (2017). Current state and prospects of the phytosynthesized colloidal gold nanoparticles and their applications in cancer theranostics. *Applied Microbiology and Biotechnology, 101,* 3551–3565

Pelaez, M., Nolan, N.T., Pillai, S.C., Seery, M.K., Falaras, P., Kontos, A.G., Dunlop, P.S.M., Hamilton, J.W.J., Byrne, J.A., Shea, K., Entezari, M.H., & Dionysiou, D.D.

(2012). A review on the visible light active titanium dioxide photocatalysts for environmental applications. *Applied Catalysis B: Environmental, 125*, 331– 349

Peral, J., Domenech, X., & Ollis, D. F. (1997). Heterogeneous photocatalysis for purification, decontamination and deodorization of air. *Journal of Chemical Technology and Biotechnology, 70,* 117-140

Pierre, A.C. (1998). *Introduction to Sol-Gel processing.* London: Kluwer Academic Publishers.

Quan, F., Hu, Y., Zhang, X., & Wei, C., (2014). Simple preparation of Mn-N-codoped $TiO_2$ photocatalyst and the enhanced photocatalytic activity under visible light irradiation. *Applied Surface Science, 320,* 120–127

Roy, R. (1987). Ceramics by the solution-sol-gel route. *Science, 238* (4834), 1664 – 1669

Salavati, M., Davar, F., & Mir, N. (2008). Synthesis and characterization of metallic copper nanoparticles via thermal decomposition. *Polyhedron, 27,* 3514–8

Samokhvalov, A. (2017). Hydrogen by photocatalysis with nitrogen codoped titanium dioxide. *Renewable and Sustainable Energy Reviews, 72,* 981–1000

Sayılkan, F. (2007). *Nano-$TiO_2$ fotokatalizör sentezi ve fotokatalitik aktivitesinin belirlenmesi.* Doctoral Thesis, İnönü University, Malatya

Schodek, D.L., Ferreira, P., & Ashby, M.F. (2009). *Nanomaterials, nanotechnologies and design.* United Kingdom: Butterworth-Heinemann

Senthilnathan, J., & Philip, L. (2010). Photocatalytic degradation of lindane under UV and visible light using N-doped $TiO_2$. *Chemical Engineering Journal, 16,* 83–92

Shannon, R.D. (1976). Revised effective ionic radii and systematic studies of interatomic distances in halides and chalcogenides. *Acta Crystallographica, 32,* 751–767

Sun, H., Zhou, G., Liu, S., Ang, H. M., Tadé, M., & Wang, S. (2013). Visible light responsive titania photocatalysts codoped by nitrogen and metal (Fe, Ni, Ag, or Pt) for remediation of aqueous pollutants. *Chemical Engineering Journal, 231*, 18–25

Suryanarayana, C. (1995). Nanocrystalline materials. *International Materials Review, 40,* 41 - 64

Tai, C.Y., Tai, C., Chang, M., & Liu, H. (2007). *Synthesis of Magnesium Hydroxide and Oxide Nanoparticles Using a Spinning Disk Reactor,* 5536–5541

Thomas, S. C., Sharma, H., Mishra, P. K., & Talegaonkar, S. (2015). Ceramic nanoparticles: fabrication methods and applications in drug delivery. *Current Pharmaceutical Design, 21,* 6165-6188

Wu, J.C.S., & Chen, C.H. (2004). A visible-light response vanadium-doped titania nanocatalyst by sol–gel method. *Journal of Photochemistry and Photobiology A: Chemistry, 163,* 509–515

Xu, J., Dai, W., Li, J., Cao, Y., Li, H., He, H., & Fan, K. (2008). Simple fabrication of thermally stable apertured N-doped $TiO_2$ microtubes as a highly efficient photocatalyst under visible light irradiation. *Catalysis Communications, 9,* 146–152

Xu, Q., & Anderson, M.A. (1994). Sol–gel route to synthesis of microporous ceramic membranes: preparation and characterization of microporous $TiO_2$ and $ZrO_2$ xerogels. *Journal of the American Ceramic Society, 77* (7), 1939–1945

Yamamoto, T. (2002). Rutile and anatase mixed crystal $TiO_2$ thin films prepared by pulsed laser deposition. *Thin Solid Films,* 420 –421, 100–106

Yang, J., Bai, H., Tan, X., & Lian, J. (2006). IR and XPS investigation of visible-light photocatalysis nitrogen–carbon-doped $TiO_2$ film. *Applied Surface Science, 253,* 1988–1994

Yoder, C.H. (2006). *Ionic compounds: Applications of chemistry to mineralogy*. Wiley: Wiley, John, & Sons, Inc, 17

Yuan, Z., Jia, J., Zhang, L. (2002). Influence of co-doping of Zn(II)+Fe(III) on the photocatalytic activity of $TiO_2$ for phenol degradation. *Materials Chemistry and Physics, 73,* 323–326

Zaleska, A., Sobczak, J.W., Grabowska, E., & Hupka, J. (2008). Preparation and; photocatalytic activity of boron-modified $TiO_2$ under UV and visible light. *Applied Catalysis B: Environmental, 78,* 92–100

Zhang, H., Liang, Y., Wu, X., & Zheng, H. (2012). Enhanced photocatalytic activity of (Zn, N)-codoped $TiO_2$ nanoparticles. *Materials Research Bulletin, 47,* 2188–2192

Zhao, Y. F., Li, C., Lu, S., Liu, R. X., Hu, J. Y., Gong, Y.Y., & Niu, L. Y. (2016). Electronic, optical and photocatalytic behavior of Mn, Ndoped and co-doped $TiO_2$: Experiment and simulation. *Journal of Solid State Chemistry, 235,* 160–168

Zhu, J., Zheng, W., He, B., Zhang, J., & Anpo, M. (2004). Characterization of Fe-$TiO_2$ photocatalysts synthesized by hydrothermal method and their photocatalytic reactivity for photodegradation of XRG dye diluted in water. *Journal of Molecular Catalysis A: Chemical, 216,* 35–43